QATAR UNIVERSITY

COLLEGE OF ENGINEERING

STRENGTHENING OF SHEAR DEFICIENT REINFORCED CONCRETE BEAMS USING NEAR SURFACE EMBEDDED FABRIC REINFORCED CEMENTITIOUS MATRIX

BY

TADESSE GEMEDA WAKJIRA

A Thesis Submitted to

the Faculty of the College of

Engineering

in Partial Fulfillment

of the Requirements

for the Degree of

Masters of Science in Civil Engineering

June 2018

© 2018. Tadesse Gemeda Wakjira. All Rights Reserved.

COMMITTEE PAGE

The members of the Committee approve the Thesis of Tadesse Gemeda Wakjira defended on 09/05/2018.

_____

Dr. Usama Ebead
Thesis Supervisor

_____

Dr. Khaled Galal
Committee Member

_____

Dr. Mohammed Elshafie
Committee Member

_____

Dr. Alaa Al-Hawari
Committee Member

Approved:

_____

Khalifa Al-Khalifa, Dean, College of Engineering

ABSTRACT

WAKJIRA, TADESSE, G., Masters :

June : 2018, Masters of Science in Civil Engineering

Title: Strengthening of Shear Deficient Reinforced Concrete Beams Using Near Surface Embedded Fabric Reinforced Cementitious Matrix

Supervisor of Thesis: Usama, A, Ebead.

This thesis presents an experimental study on the efficacy of new concepts of strengthening reinforced concrete beams deficient in shear. The first concept is referred to as "near surface embedded" fabric reinforced cementitious matrix (NSE-FRCM). The interaction between the transverse shear reinforcement (TSR) and NSE-FRCM system has been investigated. The second concept, which is a combination of the NSE-FRCM and externally bonded FRCM is also investigated and can also be referred to as hybrid "near surface embedded/ externally bonded" NSE/EB-FRCM system. The experimental program included construction and testing of twenty medium-scaled RC beams. Two beams were kept unstrengthened to act as references, while twelve beams were strengthened using the NSE-FRCM technique and the remaining six beams were strengthened using the hybrid NSE/EB-FRCM. For the NSE-FRCM technique, six beams were reinforced in shear with 6 mm diameter steel bars spaced at 215 mm within the critical shear span (CSS), while the remaining six beams had no TSR. The test variables included the FRCM type (carbon FRCM, glass FRCM and polyparaphenylene benzobisoxazole FRCM), strengthening configuration (full and intermittent strips), and presence of TSR within the CSS (for the NSE-FRCM technique). The test results revealed that both NSE-FRCM and hybrid NSE/EB-FRCM techniques can be used to significantly enhance the shear behavior of RC

beams. Moreover, the NSE-FRCM system has shown to be a promising alternative to the conventional externally bonded FRCM system with the advantage of reducing the tendency to debonding of FRCM off the concrete substrate. Finally, an analytical approach has been proposed based on the simplified compression field theory (SCFT) to predict the ultimate load carrying capacity of RC beams strengthened in shear using FRCM system. A database of over sixty RC beams strengthened in shear using different FRCM fabric types, obtained from the literature, has been used to validate the proposed model.

ACKNOWLEDGMENTS

First and foremost, I would like to thank the Almighty God for his unending blessings and mercy. I am grateful to my supervisor, Prof. Usama Ebead, for his consistent support, expert guidance and immense knowledge that helped me during this research work and writing the thesis. The door to Prof. Usama Ebead office was always open whenever I ran into a trouble or had a question. His consistent support and guidance made this work feasible. I would also like to thank Eng. Siju Joseph, Lab Technician, for his support in carrying out the experimental work. Finally, my deepest gratitude goes to my family for their love and prayers.

TABLE OF CONTENTS

LIST OF TABLES

LIST OF FIGURES

NOTATION AND SYMBOLS

B	Basalt
C	Carbon
C-FRCM	Carbon fabric reinforced cementitious matrix
CSS	Critical shear span
EB	Externally bonded
FRCM	Fabric reinforced cementitious matrix
FRP	Fiber reinforced polymer
G-FRCM	Glass fabric reinforced cementitious matrix
LVDT	Linear variable displacement transducer
NSE	Near surface embedded
NSM	Near surface mounted
PBO	Polyparaphenylene benzobisoxazole
PBO-FRCM	Polyparaphenylene benzobisoxazole fabric reinforced cementitious matrix
RC	Reinforced concrete
TSR	Transverse shear reinforcement
W/C	Water–cement ratio
ρ_{sx}	Reinforcement ratio of flexural tensile bars
f_c'	Compressive strength of concrete
ε_x	Strain in the longitudinal tensile reinforcement

a_f	Area of FRCM fabric per unit width in the transverse direction
A_{sv}	Area of TSR
E_f	FRCM tensile modulus of elasticity
E_s	Elastic modulus of steel
L_{CSS}	FRCM strip width
P_u	Ultimate load carrying capacity
S_x	Vertical distance between the longitudinal reinforcement
S_{xe}	Crack spacing
v_f	Shear strength of FRCM
v_s	Shear strength of TSR
v_c	Shear strength of concrete
$a_{f,warp}$	Area of the fabrics per unit width in the warp direction
$a_{f,weft}$	Area of the fabrics per unit width in the weft direction
a_g	Maximum aggregate size
d	Effective depth of the section
f_1	Diagonal tension stress
f_2	Diagonal compression stress
f_f	Effective tensile strength of FRCM
f_{sv}	Yield strength of TSR
δ_u	Deflection at the ultimate load
$\varepsilon_{FRCM,U}$	FRCM strains at the ultimate load

$\varepsilon_{c,u}$	Compressive strain developed in concrete at the ultimate load
ε_f	Effective tensile strain of FRCM
$\varepsilon_{s,u}$	Strain developed in flexural bar at the ultimate load
ρ_f	Reinforcement ratio of FRCM
ρ_{SV}	Reinforcement ratio of TSR
C/C	Center to center spacing
Ø	Steel bar diameter
Ψ	Energy absorption
α	Angle of inclination
β	Tensile stress factor in the cracked concrete
ν	Shear stress
K_f	Axial rigidity of FRCM system

CHAPTER 1: INTRODUCTION

This chapter addresses the hypothesis and research problems, aims and objectives, methodology and structure of the thesis.

1.1. Hypothesis and Research Problems

Nowadays, there exists an increasing demand for the strengthening of structures because of their deterioration caused by ageing, severe environmental conditions such as hurricane, design limitations and design and/or construction errors. The existing literature has shown successful applications of fabric reinforced cementitious matrix (FRCM) composites for the strengthening of reinforced concrete (RC) beams when externally bonded to the surface of the concrete. However, the high strength FRCM composite utilization to its full capacity has been limited due to the debonding of externally bonded (EB) FRCM system off the concrete substrate [1–4]. There is a high tendency of the externally bonded FRCM debonding particularly for thicker FRCM system. To mitigate this problem, an alternative method of FRCM application that is referred to as "near surface embedded" FRCM (NSE-FRCM) is introduced. Three different types of FRCM composites are used; namely, carbon, glass and polyparaphenylene benzobisoxazole (PBO). The present work may reveal that the NSE-FRCM technique is an effective way to mitigate the debonding type of failure that is often associated with the EB counterpart. The NSE technique is limited to a certain number of fabric layers that can be embedded within the concrete cover. As a solution to such an issue, another form of the hybrid NSE and EB technique that is referred to as hybrid "near surface embedded/ externally bonded" NSE/EB-FRCM technique has been introduced.

1.2. Aims and Objectives of the Study

This research generally aimed to introduce a new form of NSE-FRCM technique for the strengthening of RC beams deficient in shear.

The specific objectives are:

- To study the efficacy of the NSE-FRCM and hybrid NSE/EB-FRCM techniques in enhancing the ultimate load carrying capacity of RC beams.
- To investigate the effectiveness of different types of FRCM system.
- To investigate the influence of various configurations of FRCM on the load carrying capacity and deformational characteristics of the strengthened beams.
- To investigate the interaction between the NSE-FRCM system and the transverse shear reinforcement (TSR).
- To investigate the failure mechanisms of the beams strengthened with NSE-FRCM and hybrid NSE/EB-FRCM techniques.
- To propose an analytical model, based on the simplified compression field theory (SCFT), to predict the ultimate load carrying capacity of FRCM strengthened beams.

1.3. Methodology

Experimental tests have been carried out on twenty (20) medium-scaled RC beams of dimensions 2100 × 150 × 330 mm (length × width × height). Three test parameters are investigated; namely, (a) FRCM type: glass FRCM (G-FRCM), carbon FRCM (C-FRCM), and PBO-FRCM, (b) strengthening configuration: full versus intermittent configuration, and (c) number of FRCM layers. In addition to this, the interaction between the FRCM and

TSR has been studied for the NSE-FRCM system. The beam testing was carried out using Universal Testing Machine (UTM) under three-point loading at a displacement rate of 0.25 mm/min. The experimental results were mainly investigated in terms of the ultimate load carrying capacity, deformational characteristics, failure modes and strain results.

1.4. Structure of the Thesis

Chapter 2: Background and Literature Review – a comprehensive literature review and background on the strengthening of RC beams is presented in this chapter.

Chapter 3: Experimental Program – material properties, test matrix, specimen description and preparation, strengthening procedures, test setup and instrumentations, and testing procedures are presented under this chapter.

Chapter 4: Results and Discussion – experimental results in terms of the load carrying capacity, deflection, crack width, load–deflection responses, failure modes, strains, and the influence of different test variables on the strengthening performance of the FRCM system are discussed under this chapter.

Chapter 5: Analytical Formulation – theoretical model based on the simplified compression field theory is proposed to predict the ultimate load carrying capacity of RC beams strengthened in shear using FRCM system.

Chapter 6: Summary and Conclusion – summary of this research study, the main findings and conclusions that can be drawn from this study are presented. The chapter closes with recommendations for future work.

PUBLICATIONS

Journal Papers

1. Wakjira T, Ebead U. Hybrid NSE/EB technique for shear strengthening of reinforced concrete beams using FRCM: Experimental study. Constr Build Mater 2018;164:164–77. doi:10.1016/j.conbuildmat.2017.12.224.
2. Wakjira T, Ebead U. FRCM/internal transverse shear reinforcement interaction in shear strengthened RC beams. Comp Struc (Manuscript submitted).

Conference Papers

1. Effectiveness of FRCM system in strengthening of RC beams in shear using hybrid NSE/EB technique: ISEC EURO MED SEC 2 (paper accepted).
2. An effective Technique Utilizing FRCM System in Strengthening RC Beams in Shear: ISEC EURO MED SEC 2 (paper accepted).
3. Behavior of RC beams strengthened in shear using near surface embedded FRCM: CONCET2018 (paper accepted).
4. A new approach for predicting the shear capacity of FRCM strengthened RC beams in shear: CONCET2018 (paper accepted).
5. Efficacy of FRCM systems in flexural strengthening of RC T-beams: CONCET2018 (paper accepted)
6. FRCM/stirrups interaction in RC beams strengthened in shear using NSE-FRCM: CONCET2018 (paper accepted).

CHAPTER 2: LITERATURE REVIEW

The chapter begins with a brief introduction to the strengthening of structures and provides a review on the available strengthening materials and methods. A general introduction and a review of the selected literature on the applications of the FRCM system for the flexural and shear strengthening of RC beams has been provided herein.

2.1. Strengthening of Structures

Concrete being the most versatile construction material and possessing several advantages over other construction materials, is widely used all over the world. Concrete structures, sometimes, become structurally deficient and/or deteriorated. The corrosion of reinforcing steel bars is the main cause of such structural deterioration. Other causes of structural deterioration include changes in functionality that may lead to an increase in the service load. A structure may also be subjected to blast damage, structural damage caused by severe environmental conditions such as fire, hurricane and seismic events, design errors, construction errors, and ageing of the structure. The events also require the decision maker to remedy their deleterious effects. In order to overcome these effects, there are two options, i.e., reconstruction after demolition or strengthening. Structural strengthening is preferred over reconstruction after demolition as the former is most likely cost effective. Moreover, some of the structures may have historical and cultural values that make them undesirable for demolition.

Structural strengthening is used to enhance the capacity of the structural element to carry loads greater than its design load, restore the capacity of the damaged structural elements, or reduce the deflection caused by overloading of structural members.

Nowadays, numerous structural strengthening techniques are available. A brief summary of the selected available techniques is discussed below classifying them into traditional and advanced strengthening system.

2.1.1. Traditional Strengthening Systems

These systems use concrete and/or steel for the strengthening of the structural elements. Some of the traditional strengthening systems include section enlargement, internal/external post-tensioning, and span shortening. Section enlargement involves casting of additional concrete to an existing structural element to increase the flexural, shear, torsion, or axial capacity of the structural element. It can be used to enhance the load carrying capacity of the structural element including beam, slab, column, and wall. RC jacketing is the most frequently used section enlargement method to strengthen columns by increasing their axial strength and stiffness. There are some drawbacks associated with RC jacketing including additional weight due to the newly added concrete, loss of space, and longer time of installation. Figures 1a through 1c show the general procedures for RC column jacketing.

a) Chipping of existing column face

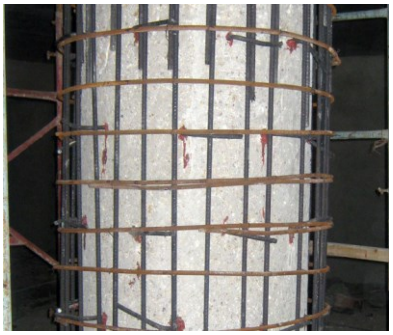

b) Installation of additional reinforcement

c) Formwork installation and casting concrete

Figure 1: RC column jacketing [5].

Internal/external post-tensioning involves application of post-tensioned forces to resist new loads [6]. Pre-stressed tendons or steel bars with high strength placed outside of the section (external post-tensioning) or inside of the original section (internal post-tensioning) are used to deliver the forces as shown in Fig. 2 and Fig. 3, respectively.

Figure 2: Strengthened headstocks of Tenthill Creek bridge by external post-tensioning [6].

Figure 3: Internal post-tensioning of beam [7].

Finally, span shortening is a reduction of the span length of an existing element by proving extra supports. The extra supports can be installed by the use of structural steel members and/or cast-in-situ RC elements. The connection between the new support and an existing member can be detailed by the use of adhesive anchors and bolts. Figures 4 shows span shortening systems used for the strengthening of parking garage slabs. However, this method may cause reduction of headroom and loss of space and thus it has a negative impact on the structural aesthetics [8].

Figure 4: Strengthening of parking garage slab by span shortening [9].

In spite of increasing the capacity of the structural elements, the traditional strengthening systems require high installation cost and are susceptible to corrosion. To overcome these drawbacks, an alternative non-corrosive advanced strengthening materials have been introduced.

2.1.2. Advanced Materials for Strengthening

Advanced materials and composites can be used for the structural strengthening of existing structures. Over the last decades, the fiber reinforced polymer (FRP) composites had gained popularity as a viable strengthening solution due to their favorable properties over those of the traditional strengthening solutions. Some of the advantages of the FRP composites include the ease and speed of application, resistance to corrosion, minimum modification in the dimension of the section and high strength to weight ratio. FRP composites have various strengthening applications including strengthening of RC beams or girders in both shear and flexure [10–16], flexural strengthening of RC slab [17,18], and column and shear wall confinement [19–21]. Different techniques of FRP application have been developed through time among which the externally bonded (EB) [22–28], near surface mounted (NSM) [29–35], mechanically fastened (MF) [36], and hybrid EB and MF [15,16] were commonly reported.

An EB-FRP has extensively used in the strengthening of RC structural members for increasing shear, flexure, axial and torsion capacity of the structural members by providing additional tension reinforcement. It involves bonding of the FRP plates or strips to the structural member using adhesive material; namely, epoxy resin and/or using mechanical anchorage system. A state of art on the anchorage of FRP system has been presented by Grelle and Sneed [37]. A MF-FRP involves anchoring the ends of dry FRP material on the structural member [36]. On the other hand, a NSM-FRP system involves application of the strengthening material; namely, FRP rods or strips with an appropriate adhesives (usually epoxy resin) into grooves in concrete cover of the structural member [31–33]. The use of NSM technique in FRP strengthening system has shown to be effective

in both FRP bar [30,33,38–40] and sheet or strip [29,30,32,41] forms. Some of the advantages of this technique include maintaining the aesthetics of the strengthened element and better protection of the strengthening material from any external damage. It can also be used for replacing removed spalled concrete for beams severely damaged due to corrosion. Moreover, the NSM technique can be used to reduce the chance of debonding modes of failure [42,43]. This mode of failure being the governing failure mode in EB technique limits the full utilization of the strengthening material.

Despite their effectiveness relative to the traditional strengthening methods, FRP composites possess some drawbacks owing to the reliance on epoxy adhesives. Some of these drawbacks include the incompatibility with the concrete [44], susceptibility to failure at high temperatures [45,46], and inability to apply on wet surfaces [44,47]. In order to partially alleviate these problems, fabric reinforced cementitious matrix (FRCM) strengthening system has been introduced as an alternative to the FRP counterpart [48–51]. FRCM composites may be regarded as more advantageous when compared to the FRP composite materials [4,52–55] due to their compatibility with the concrete substrate. In addition, FRCM composites possess good resistance to elevated temperatures and fire [45,46], while being able to be applied at a temperature as low as 0°C [50]. The eco-friendly FRCM composites accommodate recycled cementitious materials as part of the matrix composition [48].

2.2. Fabric Reinforced Cementitious Matrix

2.2.1. General

The textile fabrics in the FRCM composite is used to carry tensile stresses, while the mortar acts as a binding agent and to transfer the stresses between the substrate and the fabrics. The commonly available fabric types are carbon, glass, PBO, and basalt fabrics. This cementitious-based strengthening system is more compatible with the concrete substrate. Si Larbi et al. [56] used epoxy resin to bond the precast FRCM plates to the RC beams. Oluwafunmilayo et al. [57] studied the shear strengthening efficacy of the FRCM system bonded to the concrete substrate by cementitious mortar compared with that of epoxy adhesive [57]. On the other hand, Contamine et al. [58] compared hand lay-up in-situ FRCM strips bonded to concrete with cement mortar and precast FRCM plate glued to the concrete substrate. In all application methods, the cement-based composites are found to be effective and a promising strengthening material for RC beams deficient in shear [4,53,59–61], flexure [1,3,51,62–64], and torsion [65] in addition to column confinement [66–68]. Moreover, it can also be used to enhance the ductility behavior [4,59,69] and increase the serviceability of beams by decreasing the crack width [70]. A review on the flexural and shear strengthening applications of FRCM system has been provided in the subsequent sections.

2.2.2. Flexural Strengthening of RC Beams using FRCM System

D'Ambrisi and Focacci [63] studied the use of FRCM system for the strengthening of RC beams in flexure. The test parameters were the type of fabric (carbon and PBO), type of matrix, and the number of fabric layers. From the experimental results, the authors concluded that PBO-FRCM performed better than that of C-FRCM, while it showed the same performance as that of carbon FRP system in terms of the enhancement in the ultimate load carrying capacity. The percentage of gain in the ultimate load carrying capacity for PBO-FRCM and carbon FRP was about 30%, while it ranged between 9% and 18% for C-FRCM beams. Moreover, the failure modes in the FRCM strengthening system were mostly governed by delamination at the fabrics and matrix interface.

Babaeidarabad et al. [71] studied the efficacy of PBO-FRCM system in flexural strengthening of RC beams tested on eighteen (18) number of rectangular RC beams. The test parameters were the number of fabric layers (one and four) and the substrate concrete strength (low and high strength). From the experimental results, it was concluded that PBO-FRCM is effective in increasing the ultimate load carrying capacity and flexural strength of the beams. For low strength concrete, the increase in the flexural capacity was about 32% and 92% for one and four layers of FRCM system, respectively. On the other hand, for high strength concrete, the increase in the flexural capacity was about 13% and 73% for one and four layers of FRCM system, respectively. Two types of failure modes were observed; namely, the fabric slippage within the matrix and the debonding of FRCM off the concrete substrate. The authors concluded that the failure mode depends on the amount of FRCM reinforcement.

Jabr et al. [72] studied the effectiveness of FRCM in flexural strengthening of RC beams tested on eight rectangular RC beams over reinforced in shear. All specimens were strengthened in flexure with two layers of FRCM system except one specimen strengthened with four layers of glass FRCM. The test variables were the internal flexural reinforcement ratio (low reinforcement ratio, 0.18ρ and medium reinforcement ratio, 0.36ρ) and fabric type (glass, carbon, and PBO). The authors classified the observed failure modes into three different types; namely, fiber slippage (Type-I failure), FRCM debonding off the concrete substrate (Type-II failure), and debonding within the FRCM matrix at fiber net layer or delamination/rupture (Type-III) failure. From the experimental results, it was concluded that PBO-FRCM system significantly increased the ultimate load carrying capacity by 25% and 33% for beams with moderate and low reinforcement ratios relative to the unstrengthened beam, respectively. However, the increase in the ultimate load carrying capacity for glass and carbon FRCM beams was less than 5%, which was mainly due to the premature bond failure as per the authors. Moreover, FRCM contribution to the load carrying capacity decreased with an increase in the internal flexural reinforcement ratio. Other scholars report similar results indicating the successful application of the FRCM system for flexural strengthening of RC beams [48,64,71,73,74].

2.2.3. Shear Strengthening of RC Beams using FRCM System

The existing literature revealed a successful application of EB-FRCM system for the strengthening of shear deficient RC beams. The shear strengthening performance of FRCM system depends on various factors including FRCM type [47,52,69], FRCM thickness or number of layers [3,4,44,47,53,57,58,75,76], wrapping scheme [3,44,52,56], geometric configuration [58,59], presence of end anchorage [49,53,70,76], strengthening orientation [47], FRCM fiber grid spacing or the amount of fibers in the grid [49,75], and substrate concrete strength [4]. In addition to these, the existence of the TSR within the CSS influence the strengthening performance of the FRCM system [57,77,78]. Literature available on the effect of TSR on the effectiveness of FRCM system has been rather limited [57,77] and has focused on the use of a single type of EB-FRCM system, i.e., carbon FRCM. The state of research on the strengthening of externally bonded FRCM (EB-FRCM) system has been presented in the work of Oluwafunmilayo et al. [2]. The factors that affect the performance of the FRCM system for the strengthening of RC beams in shear are discussed below in detail.

2.2.3.1. FRCM Stiffness

The efficacy of FRCM system depends on its stiffness, which is a function of the amount of FRCM system or the number of fabric layers in the composite and fiber grid spacing in addition to the fabric type. The performance of the FRCM system increases with an increase in its stiffness. Increasing the number of fabric layers increases the stiffness of the FRCM system, which in turn increases the load carrying capacity of the strengthened beam. In the study conducted by Triantafillou and Papanicolaou [44], increasing the

number of FRCM layers from one to two increased the ultimate load carrying capacity of the beam by 37%. Similarly, studies by Contamine et al. [58] reported that increasing the thickness of FRCM reinforcement from 5 mm to 10 mm raised the shear capacity of the beam by about 4%. Other authors reported similar results [3,4]. The change in the number of FRCM layers also found to alter the failure modes. Increasing the number of fabric layers changed the mode of failure from partial fibers rupture and slippage, which was observed in one layer to debonding of FRCM with the concrete cover [3]. According to the authors, this alteration was due to the increased bond between the strengthening system and substrate concrete as a result of an overlapping of at least two fabric layers. Similarly, according to the study conducted by Loreto et al. [4] changing the number of FRCM layer from one to four altered the mode of failure from slippage of fabric (for one layer) to debonding of FRCM from the substrate (for four layers).

Increase in the amount of fiber in the grid or decrease in the fiber grid spacing increases the FRCM stiffness which in turn increase its performance [75]. Furthermore, for intermittent FRCM configuration, wider and properly spaced strips have better performance than narrow strips. Increasing the spacing between the strips hinders the performance of the strengthening system. Moreover, reducing the strip spacing helps to decrease the number of cracks between the strips [49].

Different types of fabrics were used in the literature to investigate the efficacy of FRCM strengthening system including carbon fabric [44,52,56,58,75], glass fabric [52,56,58,70], PBO fabric [49,69,79], and basalt fabric [47,59]. In the study conducted by Azam and Soudki [52], carbon FRCM showed better performance than glass FRCM of the same quantity in both side bonded and U-wrapping schemes owing to the higher FRCM

stiffness in the former. In the test conducted by Escrig et al. [69], PBO fabric showed better performance than carbon fabric, basalt fabric and glass fabric, while basalt fabric and glass fabric showed the same performance. However, glass FRCM showed better bonding performance than basalt FRCM. On the other hand, Al-Salloum et al. [47] concluded that basalt FRCM is uneconomical for shear strengthening of beams due to its low strength and stiffness.

2.2.3.2. Wrapping Scheme

FRCM can be applied in complete wrapping, U-wrapping or side bonded scheme [3]. From the experimental results, Si Larbi et al. [56] concluded that complete wrapping has better performance than side bonded scheme. Similarly, Tetta et al. [3] concluded that complete wrapping performs better than all the other wrapping scheme, while U-wrapping has better performance than side bonded scheme. The findings of Azam and Soudki [52] showed similar behavior in terms of strength and failure mechanism between U-wrapping and side bonding. The authors concluded that unlike FRP system, in FRCM system U-wrapping is not required for sufficient FRCM/concrete bond. Moreover, Triantafillou and Papanicolaou [44] examined the utilization of FRCM in conventional wrapping scheme and helical wrapping in which different strips of fabric are wrapped spirally in opposite directions to each other. From the experimental results, it was concluded that both types of wrapping can successfully be used to enhance the shear capacity.

2.2.3.3. Transverse Shear Reinforcement (TSR)

Gonzalez-Libreros et al. [77] studied the behavior of shear deficient RC beams strengthened with externally bonded C-FRCM system. The FRCM system reduced the

TSR strains, while the increase in the TSR area reduced the strains in the FRCM system. Similar results were reported by Oluwafunmilayo et al. [57] studying the efficacy of C-FRCM in the strengthening of shear deficient RC beams with varying amount of TSR (without TSR, 6 mm diameter TSR spaced at 75 mm and 150 mm). From the experimental results, it was concluded that an increase in the amount of TSR reduced the contribution of EB-FRCM system. The gain in the shear capacity due to FRCM strengthening ranged between 110% and 145% for the specimens without TSR within the critical shear span (CSS). However, this gain ranged between 64% and 67% for specimens reinforced with 6 mm diameter TSR spaced at 150 mm. Reducing the TSR spacing to 75 mm further reduced the gain in the shear capacity to a value that ranged between 51% and 58%. The failure in all the strengthened specimens was governed by FRCM debonding with the concrete cover.

2.2.3.4. Geometric Configuration

A continuous or full configuration of FRCM shear strengthening system has better performance than intermittent configuration [1,58,59]. Ombres [59] studied the effectiveness of PBO-FRCM shear strengthening with continuous and intermittent U-wrapping configuration. From the experimental results, it has been observed that the use of intermittent strips instead of continuous configuration decreased the shear capacity of the strengthened specimen by 12%. In a similar study, Younis et al. [1] concluded that full FRCM plate performed better than intermittent FRCM configuration due to higher amount of strengthening material in the former.

2.2.3.5. Presence of End Anchorage

According to the existing literature, providing end anchorage increases the performance of FRCM system [49,53,70,76]. The strengthening system fails by debonding from the concrete surface if adequate anchoring system is not provided [70]. Thus, provision of anchorage increases the effectiveness and utilization of the strengthening material by delaying or preventing the early debonding from the concrete substrate [70]. Shear strengthening requires relatively higher anchoring techniques than flexural strengthening [70]. Brückner et al. [70] examined the use of mechanical end anchorage in shear strengthening of FRCM system. The anchors were made of 450 mm long steel section with L-shape at the upper corner of the strengthening layer by bonding them against concrete using epoxy adhesive and anchoring them on the flange of the beam with two steel tensile bars. The authors concluded that mechanical anchorage should be provided to utilize full capacity of the FRCM system. However, this was in contrast with the results reported by Younis et al. [1] in which the provision of mechanical anchorage showed insignificant effect on the shear capacity and failure mechanisms of the strengthened specimens.

2.2.3.6. FRCM Orientation

FRCM strengthening can be performed in different orientations with 45° providing the highest performance [47]. Al-Salloum [47] compared the performance of FRCM in 45° and vertical orientation. From the experimental results, it was concluded that the strengthening system with 45° orientation performed better than those with vertical orientation.

2.2.3.7. Substrate Concrete Strength

Shear strengthening performance of FRCM system is shown to be higher in the high strength concrete substrate [4]. In the study conducted by Loreto et al. [4], one and two layers of FRCM system showed respective enhancement in the ultimate load carrying capacity of 121 % and 151 % for low strength concrete (28 MPa) specimens and 126 % and 161 % for high strength concrete (40 MPa) specimens.

2.2.3.8. Adhesive Mortar

The effectiveness of FRCM shear strengthening increases as the stiffness of the adhesive mortar increases. In the study conducted by Blanksvard et al. [75], the use of mortar adhesives with low modulus of elasticity leads to premature cracking in the FRCM system compared to mortar adhesives with high stiffness. Similarly, Tetta et al. [3] reported that low tensile strength mortar results in premature failure mode in the form of either FRCM/concrete debonding or failure within the FRCM layers. However, the failure in mortar with high tensile strength is characterized by peeling of the concrete substrate due to excellent FRCM/concrete bond.

To sum up, the efficacy of FRCM for the strengthening of shear-deficient RC beams is influenced by various factors including the number of fabric layers or FRCM thickness [3,4,44,47,53,58,75,76,80], wrapping scheme [3,44,52,56], TSR [80], geometric configuration [58,59,81], presence of end anchorage [49,53,70,76], fabric orientation [47], and fabric type [7,40,46]. With regard to the fabric type, the majority of the research work has focused on the use of a single fabric type; namely, carbon [3,44,60,75,76,80], glass [70], PBO [4,49,59], or basalt [47]. The literature available on the comparison of the

efficacy among different types of FRCM techniques for shear strengthening of RC beams is scarce [1]. A comparison between two FRCM types; namely, carbon FRCM and glass FRCM, was conducted for the shear strengthening of RC beams [52,53]. A comparison was also made among the PBO, carbon, and glass FRCM techniques, for the shear strengthening of RC beams [1,69]. Increasing the number of fabric layers of FRCM results in an increase in its thickness. Strengthening with larger number of fabric layers is associated with debonding of EB-FRCM off the concrete substrate; thus, decreasing the utilization of FRCM strengthening material [2–4]. In light of the aforementioned gaps, the present study; therefore, aims at introducing an alternative method of NSE-FRCM system for the shear strengthening of RC beams using three commercially available FRCM systems; namely, PBO-, carbon-, and glass-FRCM.

CHAPTER 3: EXPERIMENTAL PROGRAM

3.1. Material Properties

3.1.1. Concrete

Ready-mixed concrete was used to cast the RC beams included in this study using the same batch to ensure that all beams have the similar characteristics. The concrete mix was comprised of 800 kg, 1100 kg, and 370 kg of sand, gravel and ordinary Portland cement, respectively in addition to 167 kg of water, for each cubic meter of concrete. Thus, the water–cement (W/C) ratio of 0.45 was adopted. Compression tests carried out on standard, 150 × 300 mm (diameter × height), concrete cylinders as per ASTM C39/C39M [82] showed an average 28-day cylindrical compressive strength of 30 MPa with a standard deviation of 1.6 MPa.

3.1.2. Steel Reinforcement

Grade 500B bars, as per BS 4449 standard [83], were utilized as reinforcement in the RC beam specimens. Reinforcement bars with diameters of 8 mm and 16 mm were used for compression and main tensile reinforcement, respectively. Bars with diameters of 6 mm and 8 mm were used for the TSR within and outside the CSS, respectively. The longitudinal tensile reinforcement bars had an average yield strength of 595 MPa and an elastic modulus of 224 GPa, while the compressive and transverse reinforcement bars had an average yield strength of 535 MPa and an elastic modulus of 207 GPa. The yield strain was 0.266% for the tensile bars and 0.258% for the transverse and compressive reinforcement bars.

Table 1

Properties of the Steel Bars

Bar Diameter (mm)	Yield stress (MPa)	Yield strain ε_y (%)	Ultimate strain ε_u (%)	Modulus of Elasticity (GPa)
6	535	0.258	12.47	207
8	535	0.258	12.47	207
16	595	0.266	9.12	224

3.1.3. FRCM Fabric

Three different commercially available fabric types were used in the FRCM strengthening system; viz., carbon, glass, and PBO fabrics. Figures 5a through 5c show the fabric types used in the FRCM strengthening system, while the geometric and mechanical properties of the fabrics are summarized in Table 2 as provided by the manufacturers [84–86]. In all the three types of the fabrics, the textile roving are aligned in two orthogonal directions. For carbon fabrics, the longitudinal (weft) and transverse (warp) roving are spaced at 10 mm and each roving has a cross-sectional area of 0.047 mm^2/mm in both the longitudinal and transverse directions. The longitudinal and transverse roving for carbon fabrics are spaced at 14 mm and 18 mm spacing, respectively. Each roving has respective cross-sectional areas of 0.066 mm^2/mm and 0.047 mm^2/mm in the longitudinal and

transverse directions. For PBO fabrics, the roving are spaced at 17 mm and 10 mm in longitudinal and transverse direction, respectively. Each roving has a cross-sectional areas of 0.0455 mm^2/mm and 0.0155 mm^2/mm in the transverse and longitudinal directions, respectively. The tensile strength of the fabric was 4.80 GPa, 2.60 GPa, and 5.80 GPa for carbon, glass and PBO fabrics, respectively. The elastic modulus of the fabric was 240 GPa, 80 GPa, and 270 GPa for carbon, glass, and PBO-fabrics, respectively. The fabrics had an ultimate elongation of 1.80%, 3.25% and 2.15% for carbon, glass and PBO-fabrics, respectively.

Table 2

Properties of the Fabrics and Mortars in the FRCM Composites

Fabric type	Spacing (C/C) weft × warp (mm)	$A_{f,warp}$ (mm^2/mm)	$A_{f,weft}$ (mm^2/mm)	Elastic modulus (GPa)	Tensile strength (GPa)	Ultimate strain (%)	28-day compressive strength of the mortar (MPa)
Carbon	10 x 10	0.047	0.047	240	4.80	1.80	20
Glass	14 x 18	0.047	0.066	80	2.60	3.25	40
PBO	17 x 10	0.0455	0.0155	270	5.80	2.15	30

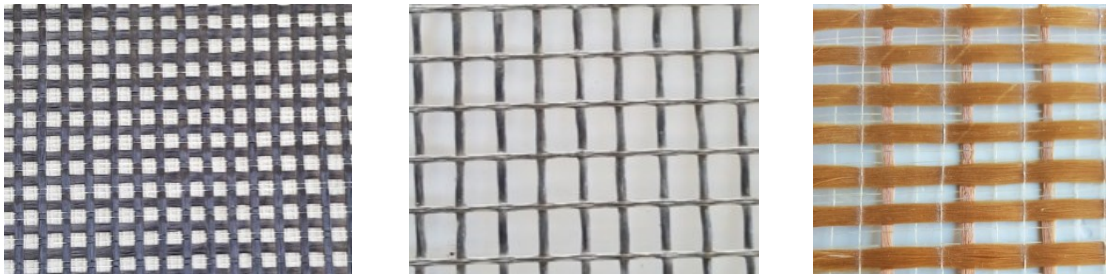

(a) Carbon fabric (b) Glass fabric (c) PBO fabric

Figure 5: Fabric types used in the study.

3.1.4. FRCM Mortar

The mortars used for the preparation of FRCM composites were RUREDIL X MESH GOLD [84], RUREDIL X MESH C10 [86], and Monotop-722 Mur [85] for PBO-FRCM, carbon FRCM, and glass FRCM, respectively. The mortar mix uses a water–cement ratio of 0.2 by weight of glass FRCM and 0.28 by weight of carbon FRCM and PBO-FRCM.

3.2. Test Specimens and Test Matrix

The test matrix is provided in Table 3. Twenty (20) medium-scaled RC rectangular beams of dimension 2100 × 150 × 330 mm (length × width × height) were fabricated and tested under three-point loading. Two beams without FRCM strengthening were used as references. The remaining eighteen (18) specimens were strengthened for shear using the FRCM system, twelve (12) specimens among which were strengthened using the NSE-FRCM technique, while the remaining six (6) specimens were strengthened using the

hybrid NSE/EB-FRCM technique as listed in Table 3. The strengthening system in the NSE-FRCM system used two layer of fabrics in the FRCM composite, while the hybrid NSE/EB-FRCM system used four layers of fabrics in the FRCM composite. Preliminary design of the strengthened beams substantiated the beam dimensions, internal reinforcement, and strengthening configuration parameters, such as the spacing between the discontinuous FRCM strips and the strengthening zone width.

For the NSE-FRCM specimens without TSR within the CSS, the beam designation used "X-Y" nomenclature as listed in Table 3 in which "X" denotes the fabric type (G- for glass, P- for PBO, and C- for carbon) and "Y" denotes the strengthening configuration ("I" represents intermittent strips and "F" represents full FRCM plate). For the NSE-FRCM specimens with TSR, the beams were designated in a similar way as those without TSR with "S" added at the end to indicate the presence of TSR within the CSS as listed in Table 3. Accordingly, G-I-S denotes a test beam strengthened with two layers of intermittent strips of G-FRCM and internally reinforced with TSR within the CSS, while C-F denotes a beam without TSR within the CSS and strengthened with full strips of C-FRCM.

The beam designation for the hybrid NSE/EB-FRCM system followed two key parameters, namely; fabric type and FRCM configuration for both near surface embedded and EB-FRCM system. The specimen designation is labelled using "A-B-D" format as shown in Table 3. "A" denotes the fabric type; "B" and "D" denotes the strengthening configuration for near surface embedded and EB-FRCM system, respectively. Accordingly, C-F-F denotes a test specimen strengthened with carbon hybrid NSE/EB-FRCM system in which both the near surface embedded and the externally bonded parts are in full configuration form.

Table 3

Test Matrix of the Beam Specimens

S.N.	Specimen ID	TSR within the CSS	Fabric type	Strengthening configuration		Number of FRCM layers	
				NSE	EB	NSE	EB
1	R	-	-	-	-	-	-
2	R-S	Ø6 C/C 215	-	-	-	-	-
3	C-F	-	Carbon	Full	-	2	-
4	C-F-S	Ø6 C/C 215	Carbon	Full	-	2	-
5	C-I	-	Carbon	Intermittent	-	2	-
6	C-I-S	Ø6 C/C 215	Carbon	Intermittent	-	2	-
7	P-F		PBO	Full	-	2	-
8	P-F-S	Ø6 C/C 215	PBO	Full	-	2	-
9	P-I	-	PBO	Intermittent	-	2	-
10	P-I-S	Ø6 C/C 215	PBO	Intermittent	-	2	-
11	G-F	-	Glass	Full	-	2	-
12	G-F-S	Ø6 C/C 215	Glass	Full	-	2	-
13	G-I	-	Glass	Intermittent	-	2	-
14	G-I-S	Ø6 C/C 215	Glass	Intermittent	-	2	-
15	C-F-F	-	Carbon	Full	Full	2	2
16	C-I-F	-	Carbon	Intermittent	Full	2	2
17	P-F-F	-	PBO	Full	Full	2	2
18	P-I-F	-	PBO	Intermittent	Full	2	2
19	G-F-F	-	Glass	Full	Full	2	2
20	G-I-F	-	Glass	Intermittent	Full	2	2

The NSE-FRCM specimens were divided into two groups with six number of strengthened beams in each group. The first group has no TSR along the CSS, while the specimens in the second group were reinforced with 6 mm diameter TSR spaced at 215 mm within the CSS as shown in Figs. 6a and 6b, respectively. The hybrid NSE/EB-FRCM specimens had no TSR within the CSS as listed in Table 3. All tested beams were designed to fail in shear within the CSS and adequate TSR, Ø8 C/C 100 mm, was provided outside the CSS as shown in Figs. 6a and 6b. The efficacy of the strengthening system is strongly influenced by the longitudinal reinforcement ratio. In the case of externally bonded FRP system, decreasing the amount of longitudinal reinforcement increases the effectiveness of FRP system [87]. Thus, to avoid the effect of longitudinal reinforcement ratio on the shear capacity of the beams by dowel action, it was kept constant in all specimens. The longitudinal tensile reinforcement used three number of 16 mm diameter tensile bars, while two number of 8 mm diameter bars were provided as compression reinforcement as shown in Fig. 6c. A constant value of 34 mm concrete cover was provided in each beam, yielding a typical beam effective depth of 280 mm as shown in Fig. 6c.

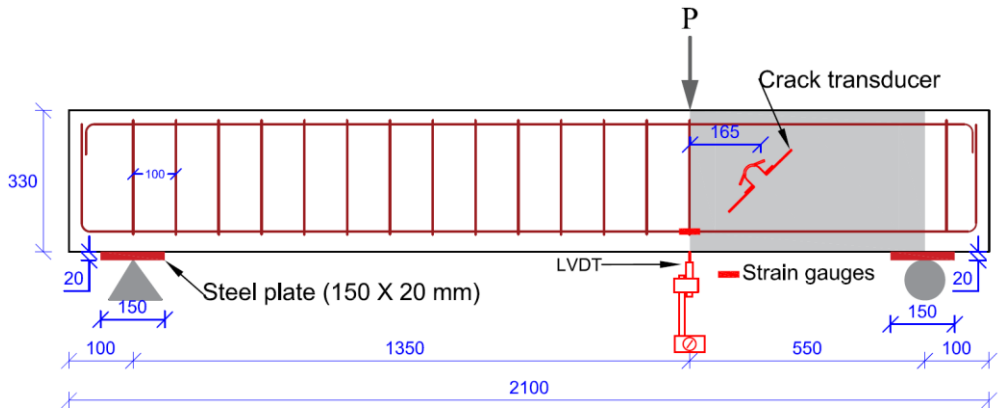

(a)

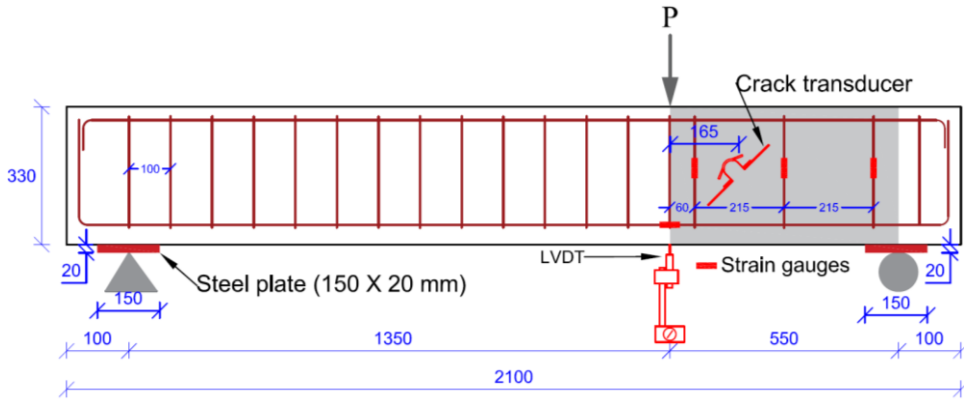

(b)

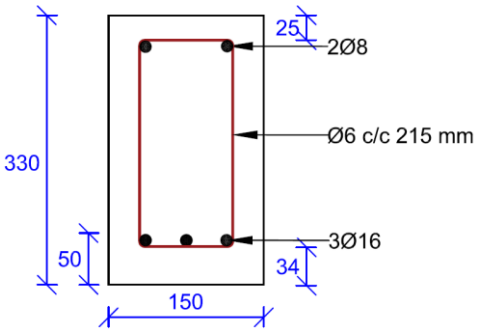

(c)

Figure 6: Longitudinal detail for specimens (a) without TSR within the CSS, (b) with TSR within the CSS, and (c) cross-sectional details at mid-span (all dimensions are in mm).

For the NSE-FRCM technique, each strengthened specimen utilized two layers of fabrics in the FRCM composites. Figures 7a and 7b show schematic of the NSE-FRCM strengthening configuration details, while Figs. 8a and 8b show the cross-sectional detail within the CSS for the NSE-FRCM and the hybrid NSE/EB-FRCM specimens, respectively. The hybrid NSE/EB-FRCM technique used two layers of near surface embedded FRCM and two more layers of EB-FRCM with different strengthening configurations, resulting in a total of four (4) layers of FRCM as shown in Fig. 8b.

The test variables are summarized as follows:

i. Type of FRCM system: Three different FRCM systems were used; namely, PBO-FRCM, carbon FRCM, and glass FRCM.

ii. Strengthening configuration: A full strengthening configuration versus intermittent strips of FRCM system as shown in Figs. 7a and 7b. The intermittent FRCM configuration involved 120 mm wide strips spaced at 95 mm within the CSS as shown in Fig. 7b. The hybrid NSE/EB-FRCM utilized two FRCM layers installed in the groove (in either full or intermittent FRCM configuration) and two more EB-FRCM layers (in full configuration) as shown in Figs. 9a and 9b.

iii. Presence of TSR (for the NSE-FRCM system): Beams with and without TSR within the CSS as shown in Figs. 6a and 6b, respectively.

iv. The effect of additional two layers of EB-FRCM system on the NSE-FRCM system.

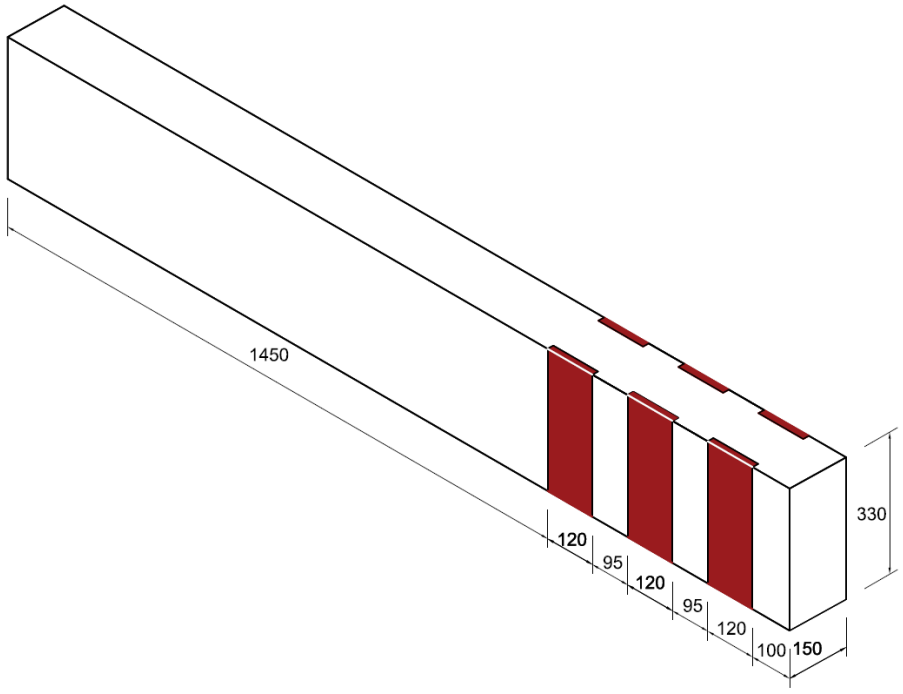

(a)

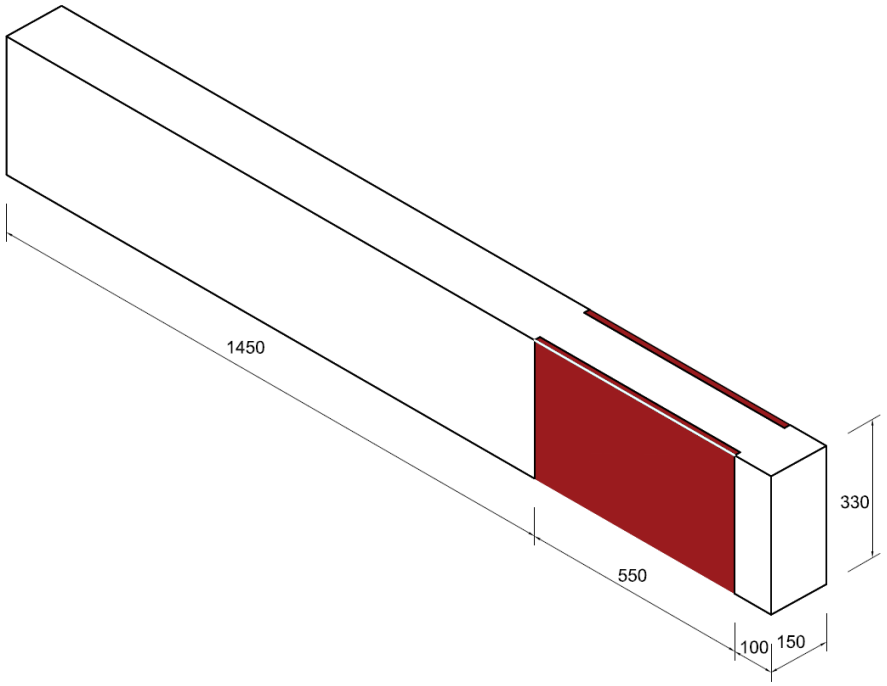

(b)

Figure 7: FRCM configuration for: (a) full FRCM plate and (b) intermittent FRCM strips (all dimensions are in mm).

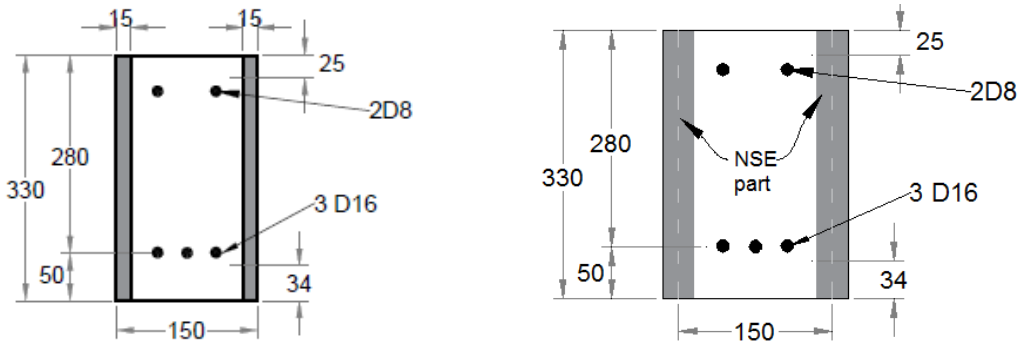

(a) NSE-FRCM strengthened beam (without TSR).

(b) Hybrid NSE/EB-FRCM strengthened beam.

Figure 8: Cross-sectional details in the CSS (all dimensions are in mm).

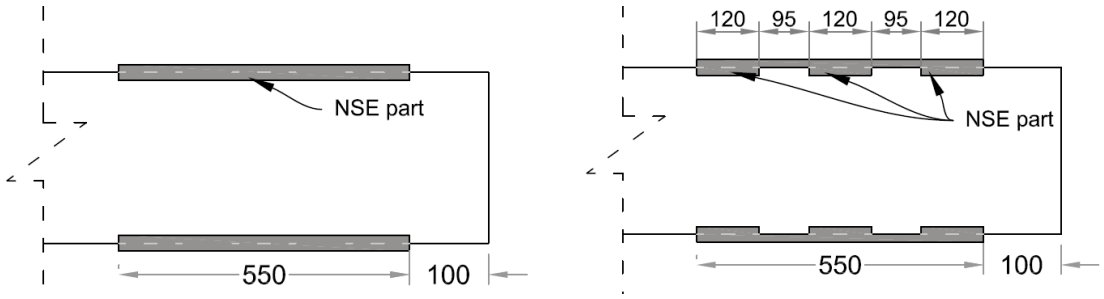

(a) Top view of full strengthening configuraiton for both EB and NSE.

(b) Top view of full configuration EB and intermittent NSE.

Figure 9: FRCM strengthening configuration detail for the hybrid NSE/EB-FRCM (all dimensions are in mm).

3.3. Preparation of Beam Specimens

The preparation of the beam specimens is discussed in detail in this section.

3.3.1. Steel Cage Preparation, Concrete casting and Curing

Preparation of the steel cage and the formwork

Based on the design shop drawings the bar bending schedule has been prepared and used to prepare the steel cages as shown in Fig. 10. The steel strain gauges for the longitudinal tensile reinforcement bars and TSR within the CSS (for specimens with TSR) have been installed after preparation of the strain gauges locations as shown in Fig. 11.

Figure 10: Preparation of the steel cages.

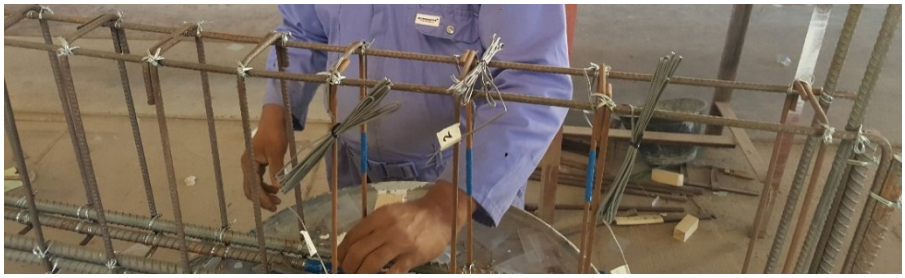

Figure 11: Installation of the strain gauges.

Preparation of formwork

The wooden formwork has been prepared in accordance with the designed beam dimensions as shown in Fig. 12.

Figure 12: Preparation of the formwork.

Concrete casting and curing

Following the preparation of the formwork, the steel cages have been placed into the prepared formwork as shown in Fig. 13a. Figure 13b shows concrete casting and surface finishing for the beam specimens.

(a) Installation of rebar cage in the formwork.

(b) Concrete casting and concrete surface finishing.

Figure 13: Specimens fabrication.

The specimens were cured for a minimum of 28-days prior to application of the strengthening material as shown in Fig. 14.

Figure 14: Curing of the beam specimens.

3.3.2. Preparation of Roughened Grooves

Following adequate curing of the beam specimens, the location of the grooves has been marked based on the designed strengthening configuration. Then grooves of 15 mm depth were cut on both sides of the beam using a slitting tool as shown in Fig. 15a. The grooves have a width of 120 mm spaced at 90 mm within the CSS for the intermittent FRCM configuration and a width of 550 mm (full shear span) for the full FRCM configuration. To prepare each groove, multiple 20 mm wide grooves have been made as shown in Fig. 15a for full configuration. The concrete between the grooves had then been removed manually by the use of chisel and hammer as shown in Fig. 15b. The prepared groove provides the already roughened surface as shown in Fig. 15c.

(a) Continuous configuration.

(b) Removal of the concrete.

(c) Already roughened surface

Figure 15: Preparation of roughened grooves.

3.3.3. Surface Preparation

The roughness of the surface plays a great role for a good bond between the concrete substrate and the strengthening material. Brückner et al. [70] recommended a minimum of 1 mm depth of roughness. The externally bonded FRCM system requires roughening the concrete substrate to which the FRCM is applied by the means of sandblasting or water jetting [1]. On the other hand, the NSE-FRCM system grooves provided a roughened surface, as shown in Fig. 15c. The labor cost of creating the roughened grooves can be considered as equivalent to roughening the surface using sandblasting for the externally bonded FRCM counterpart. Moreover, the preparation of the roughened grooves is not associated with any hazards unlike the sandblasting process that creates a high level of noise and dust that are hazardous to the workers unless proper safety precautions are taken. The surface has then been cleaned using air blower to make it free of dust and micro-fractured parts and expose sound concrete surface. Following the cleaning of the surface, the dry concrete surface was then dampened with water to a saturated surface dry (SSD) condition with no excess water. This helps to avoid water transfer from the newly applied mortar to the old concrete and thereby prevents shrinkage phenomena on cementitious matrix caused by dehydration of fresh FRCM mortar.

3.3.4. FRCM Application

The strengthening process has been illustrated in Figs. 16a through 16c and summarized as follows.

1. Application of a thin first layer of mortar using a trowel followed by the installation of first layer of fabrics as shown in Fig. 16a.

2. Full impregnation of the fabrics: Following the fiber orientation, the fabrics net was embedded into the matrix with light pressure using a trowel to ensure proper impregnation of fabrics into the matrix as shown in Fig. 16b.
3. Application of the second layer of mortar to completely cover the fabrics. Following the same procedure, the strengthening was done until the required number of FRCM layers were obtained, i.e., 2 and 4 layers for the NSE-FRCM and the hybrid NSE/EB-FRCM, respectively. An average of 5 mm thick mortar was used between the fabric layers.
4. Finally, the surface was finished using a trowel as shown in Fig. 16c.

The specimens were sealed with heissen cloth and allowed to cure for a minimum of 28-days prior to testing as shown in Fig. 16d

a) Application of first layer of mortar

b) Installation and full impregnation fabrics

c) Surface finishing

d) Curing

Figure 16: Strengthening process.

3.4. Test Setup and Instrumentation

The testing was performed using Instron Universal Testing Machine (UTM). The details of the test setup are depicted in Figs. 17a and 17b that show a beam placed in the loading frame and a view of a beam with measuring devices and gauges, respectively. The

beams were tested as simply supported system under three-point bending test at a displacement rate of 0.25 mm/min until failure.

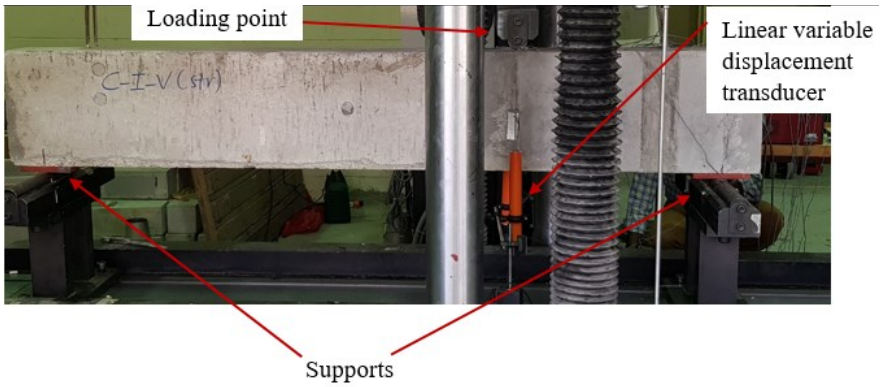

(a)

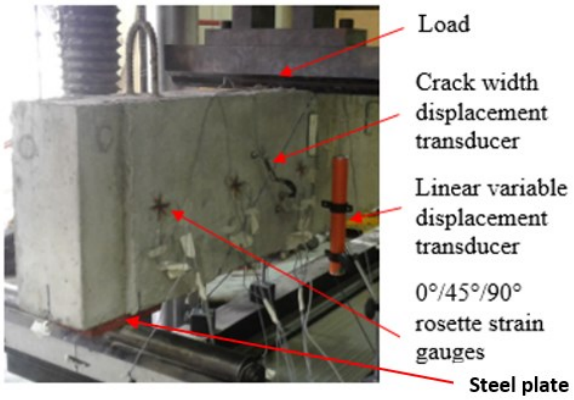

(b)

Figure 17: Test setup: (a) specimen mounted on the loading frame, and (b) a view of a specimen with measuring devices and gauges.

The following instrumentations were adopted during the test for each specimen.

3.4.1. Linear Variable Displacement Transducer

Two linear variable displacement transducers (LVDTs), located directly under the loading point, were used to measure the vertical displacement at each load step as shown in Figs. 17a and 17b.

3.4.2. Strain Gauge

The flexural strains in the tensile bars were measured with two steel strain gauges attached to the tensile reinforcement bars directly under the load location. Three more steel strain gauges were used to monitor the strains in the TSR for beams reinforced with TSR within the CSS. The steel strain gauges, FLA-5-11, had a gauge length of 5 mm and a maximum strain limit of 5%. The concrete strain gauge, PL-60-1, was used to measure the strains in the compression concrete just below the loading point. The properties of the strain gauges are given in Table 4 below as provided by the manufacturer.

Table 4

Strain Gauge Properties

Gauge Type	Application surface	Gauge length (mm)	Gauge width (mm)	Gauge factor	Strain limit (με)	Resistance (Ω)
FLA-5-11	Steel	5	1.5	2.13	50,000 (5%)	120
PL-60-11	Concrete	60	1	2.13	20,000(2%)	120

3.4.3. Strain Rosette

FRCM strains were monitored using three stacked type 0°/45°/90° rosette strain gauges, PFLR-30-11, applied on the surface of the FRCM as shown in Fig. 17b. For intermittent configuration, the rosette strain gauges were installed at the mid-span of each strip. The properties of the rosette strain used are summarized in Table 5.

Table 5

Strain Rosette Properties

Gauge Type	Application surface	Gauge length (mm)	Gauge width (mm)	Gauge factor	Strain limit (με)	Resistance (Ω)
PFLR-30-11	Concrete/Mortar	30	2.3	2.13	20,000(2%)	120

3.4.4. Crack Displacement Transducer

A clip-type displacement transducer with a capacity of ± 5 mm and gauge length of 100 mm was used to measure the crack width as shown in Fig. 17b. The crack width transducer was positioned at the middle of a line drawn from the loading point at 45-degree to the bottom of the beam, which was considered as the critical line in the literature [59]. Table 6 below summarizes the properties of the crack displacement transducer.

Table 6

Crack Displacement Transducer Properties

Type	Gauge length (mm)	Capacity (mm)	Resistance (Ω)
PI-5-100	100	±5	350

The instrumentations discussed above were connected to the data acquisition system, TML data logger, as shown in Fig. 18. Data acquisition was done at a frequency of 1 Hz.

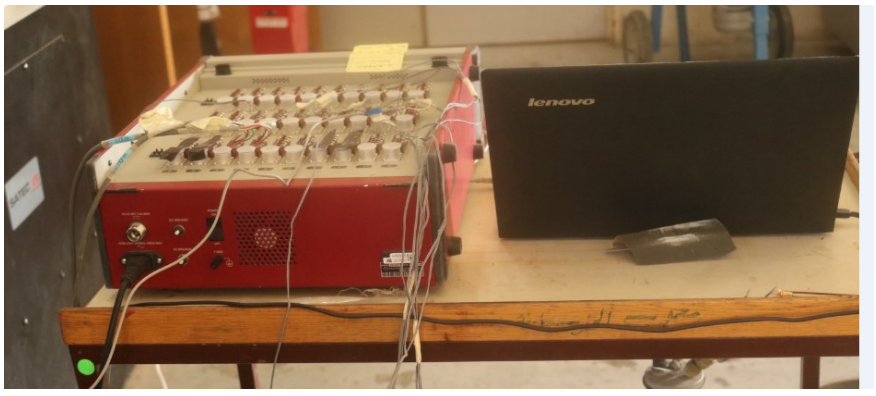

Figure 18: TML data logger.

CHAPTER 4: RESULTS AND DISCUSSION

4.1. Introduction

This chapter provides a detailed discussion on the experimental results in terms of ultimate load carrying capacity, deformational characteristics, crack width, strains developed in the tensile bars ($\varepsilon_{s,u}$), concrete ($\varepsilon_{c,u}$), and FRCM ($\varepsilon_{FRCM,u}$) at P_u, and modes of failure. The obtained result is an indication of the successful application of the FRCM strengthening system in both the NSE-FRCM and the hybrid NSE/EB-FRCM forms.

4.1.1. Test Results for NSE-FRCM

A summary of the test results for the NSE-FRCM specimens is given in Table 7 in terms of the ultimate load carrying capacity (P_u), gain in P_u, deflection at P_u (δ_u), strain developed in flexural reinforcement at P_u ($\varepsilon_{s,u}$), compressive strain developed in concrete at P_u ($\varepsilon_{c,u}$), maximum FRCM strain ($\varepsilon_{FRCM,u}$), and energy absorption (Ψ).

Table 7

Summary of the Test Result (NSE-FRCM)

1	2	3	4	5	6	7	8
Specimen ID	P_u (kN)	Gain in P_u (%)	δ_u (mm)	Ψ (kN.mm)	$\varepsilon_{s,u}$ ($\mu\varepsilon$)	$\varepsilon_{c,u}$ ($\mu\varepsilon$)	$\varepsilon_{FRCM,u}$ ($\mu\varepsilon$)
R	104	-	3.25	238	1425	-	-
C-F	184	77.1	6.48	753	2711	2036	163
C-I	176	69.3	5.16	571	1787	1142	2539
G-F	174	67.1	5.98	694	2426	1891	300
G-I	139	34.1	4.53	387	1762	1037	238
P-F	169	62.9	5.93	632	2457	1153	517
P-I	152	46.5	4.40	433	2278	1417	226
R-S	142	-	4.69	464	2000	467	-
C-F-S	208	46.0	8.72	1077	5699	1914	9061
C-I-S	199	39.7	6.00	755	3287	1660	3325
G-F-S	196	37.6	7.10	928	2768	1768	8389
G-I-S	167	17.8	6.16	643	2137	1090	2027
P-F-S	183	28.7	6.49	681	2795	1217	1215
P-I-S	162	14.3	5.95	566	2579	1042	661

4.1.1.1. Test Results for Specimens without TSR within the CSS

The reference specimen R, without TSR within the CSS, exhibited a sudden shear failure caused by a major diagonal shear cracks as shown in Fig. 19. The ultimate load recorded for R was 104 kN as listed in Table 7. The deflection of the specimen at the ultimate load was 3.25 mm as given in the fourth column of Table 7. The first crack was observed at a load of 56 kN, which was about 54% of the ultimate load. The energy absorption value of 238 kN.mm was observed for this specimen.

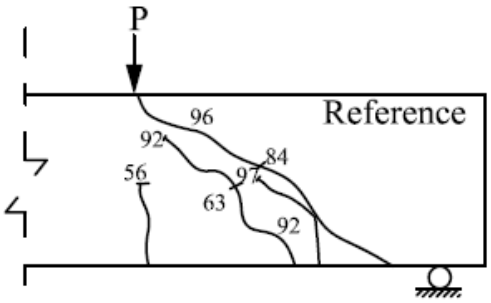

Figure 19: Crack patterns and failure modes for reference specimen, R.

Specimen C-F was strengthened with two layers of carbon NSE-FRCM in full configuration form. The ultimate load recorded for this specimen was 184 kN corresponding to 77% gain in P_u relative to R. The first crack within the CSS was observed at a load of 119 kN, which was 65% of the ultimate load. The shear capacity gradually dropped after the peak load. This specimen failed due to a crack developed between the

FRCM and concrete substrate at the bottom face, which initiated the debonding of the FRCM system as shown in Fig. 20a. However, no any sign of debonding was observed on the top face of the beam, which indicated reduced chance of debonding as shown in Fig. 20b. The maximum deflection value of 6.48 mm was observed corresponding to 99% increase in the deflection relative to the reference specimen (R = 3.25 mm). This specimen exhibited an energy absorption value of 753 kN.mm, which was more three times that for the reference specimen (238 kN.mm) as listed in Column 5 of Table 7.

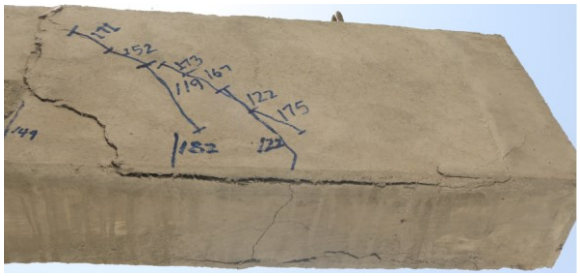

a) Bottom view

b) Top view

Figure 20: Crack patterns and failure modes for specimen C-F.

Specimen C-I was strengthened with intermittent strips of carbon NSE-FRCM system. This specimen exhibited a percentage enhancement in the ultimate load of 69% relative to the reference specimen. The shear capacity gradually dropped after the peak load. The specimen failed with a major diagonal shear crack within the CSS with no sign of debonding as shown in Fig. 21.

Figure 21: Crack patterns and failure modes for specimen C-I.

Specimen P-F, strengthened with two layers of full configuration of PBO NSE-FRCM system, exhibited the ultimate load of 169 kN corresponding to 63% gain in P_u relative to the reference specimen. The first crack within the shear span was observed at a load of 99 kN, which was 59% of the ultimate load. The load gradually dropped during the post peak load. Figures 22a and 22b show the crack patterns and failure modes of Specimen P-F. The specimen failed in shear with no any sign of debonding as shown in Figs. 22a and

22b. The maximum deflection value of 5.93 mm was observed in this specimen corresponding to 82% increase in the deflection relative to the reference specimen. The energy absorption value of 632 kN.mm was observed, which was 2.6 times the value recorded for the reference specimen.

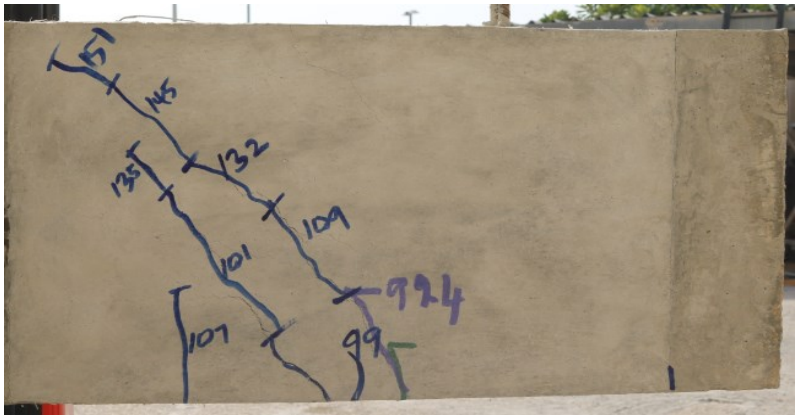

a) Critical shear span

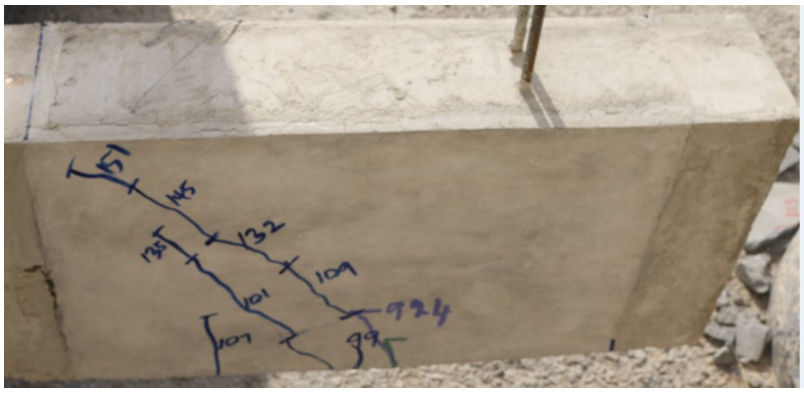

b) Top view

Figure 22: Crack patterns and failure modes for Specimen P-F.

Specimen P-I was strengthened with intermittent strips of PBO NSE-FRCM system. The percentage enhancement in P_u for this specimen was 47% relative to the reference specimen. The first crack within the shear span was observed at a load of 102 kN corresponding to 67% of the peak load (152 kN). The shear capacity gradually dropped after the peak load. The failure in this specimen was caused by a major diagonal shear cracks within the CSS as shown in Fig. 23.

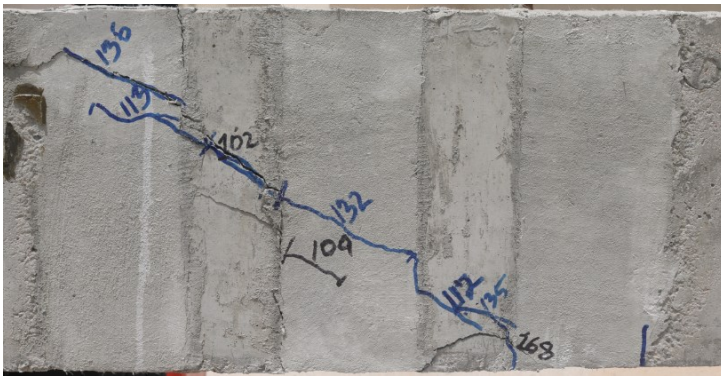

Figure 23: Crack patterns and failure modes for Specimen P-I.

Specimen G-I was strengthened with intermittent strips of glass NSE-FRCM system. This specimen showed 34% enhancement in the ultimate load carrying capacity relative to the reference specimen as given in Table 7. The first crack within the shear span was observed at a load of 85 kN corresponding to 61% of the ultimate load (139 kN). The

shear capacity gradually dropped after the peak load. The failure in this specimen was caused by a major diagonal shear cracks within the CSS with no sign of debonding.

Specimen G-F was strengthened with two layers of glass NSE-FRCM in full configuration form. The strengthening system in this specimen showed an enhancement in the ultimate load carrying capacity of 67% relative to R. The first crack was observed at a load of 66 kN, which was 38% of the ultimate load (174 kN). A gradual drop in the shear capacity was observed during the post peak load. The specimen failed with major diagonal shear cracks starting from the loading point extending to the bottom of the beam with no sign of debonding as shown in Figs. 24a and 24b. This specimen exhibited a maximum deflection of 5.98 mm corresponding to 84% increase in the deflection relative to the reference specimen. The energy absorption value of 694 kN.mm was observed, which was 2.9 times the value observed for the reference specimen as listed in Column 5 of Table 7.

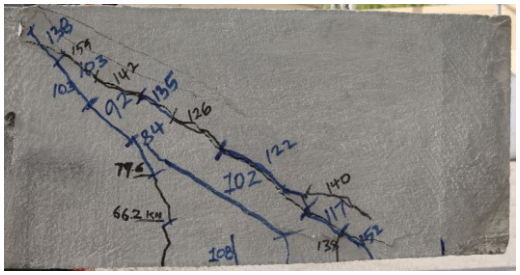

a) Critical shear span

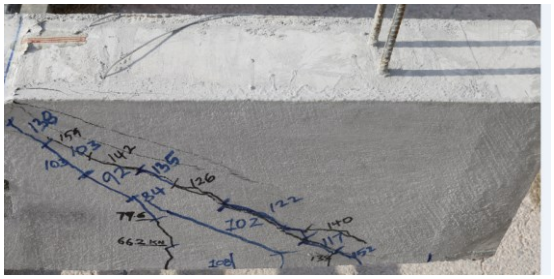

b) Top view

Figure 24: Crack patterns and failure modes for Specimen G-F.

4.1.1.2. Test Results for Specimens with TSR within the CSS

The reference specimen R-S, with TSR within the CSS, exhibited a similar failure modes as that of Specimen R; namely, sudden shear failure caused by a major diagonal shear cracks as shown in Fig. 25. The ultimate load recorded for this specimen was 142 kN as listed in Table 7. At this load, the specimen exhibited a deflection of 4.69 mm as given in Table 7. The energy absorption of 464 kN.mm was observed for this specimen as listed in Table 7.

Figure 25: Crack patterns and failure modes for reference specimen, R-S.

Specimen C-F-S showed an ultimate load of 208 kN corresponding to 46% gain in P_u relative to R-S. The shear capacity gradually dropped after the peak load. This specimen exhibited a maximum deflection of 8.72 mm, which corresponds to 86% increase in δ_u

relative to R-S. Energy absorption of 5,699 kN.mm corresponding to 132% enhancement relative to the reference specimen has been observed as listed in Column 5 of Table 7. The failure was characterized by diagonal shear failure without any signs of debonding as shown in Fig. 26.

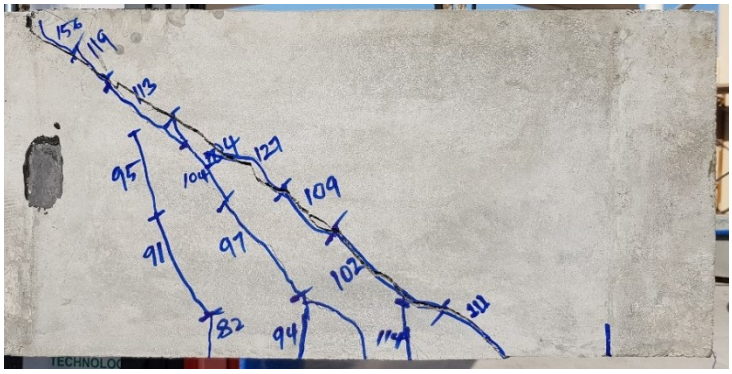

Figure 26: Crack patterns and failure modes for Specimen C-F-S.

Specimen C-I-S, strengthened with intermittent strips of carbon NSE-FRCM system, failed at an ultimate load of 199 kN corresponding to 40% enhancement in P_u relative to R-S as listed in Table 7. The shear capacity gradually dropped after the peak load. The specimen failed with major diagonal shear crack within the CSS with no sign of debonding as shown in Fig. 27.

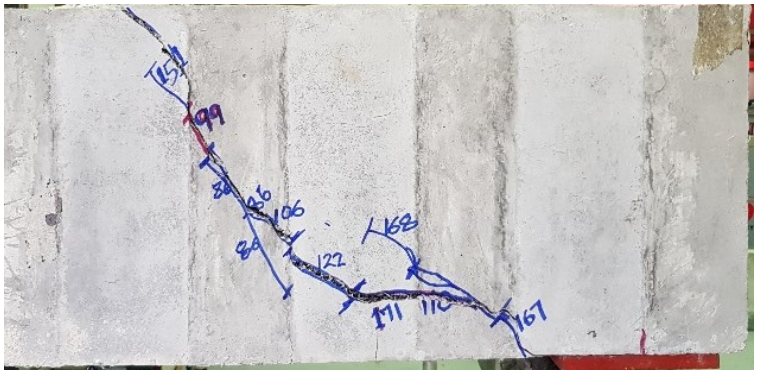

Figure 27: Crack patterns and failure modes for Specimen C-I-S.

Specimen P-F-S, strengthened with two layers of full PBO NSE-FRCM plate, failed at an ultimate load of 183 kN corresponding to 29% gain in P_u relative to R-S. A gradual drop in the shear capacity was observed during the post peak load. The specimen failed with major diagonal shear cracks without any sign of debonding. The maximum deflection for this specimen was of 6.49 mm, which was 38% higher than the value for R-S. The energy absorption of 681 kN.mm corresponding to 47% gain relative to the reference specimen was observed for this specimen as listed in Table 7.

Specimen P-I-S, strengthened with intermittent strips of PBO NSE-FRCM system, exhibited an ultiamte load carrying capacity of 162 kN corresponding to 14% enhancement in the shear capacity. The shear capacity gradually dropped after the peak load. The failure in this specimen was caused by major diagonal shear cracks within the CSS with no sign of debonding.

Specimen G-F-S was strengthened with two layers of glass NSE-FRCM in full configuration form. The strengthening system in this specimen showed an enhancement in the ultimate load carrying capacity of 38% relative to R-S. The first crack was observed at a load of 82 kN, which is 42% of the ultimate load (196 kN). A gradual drop in the shear capacity was observed during the post peak load. The specimen failed with major diagonal shear cracks without any sign of debonding as shown in Fig. 28a. The maximum deflection value of 7.10 mm was observed corresponding to 51% increase relative to R-S. The energy absorption value observed for this specimen was 928 kN.mm, which was double the value observed for the reference specimen as listed in Table 7.

Specimen G-I-S, strengthened with intermittent strips of glass NSE-FRCM, failed at an ultimate load of 167 kN, which corresponds to 18% enhancement in P_u. The shear capacity gradually dropped after the peak load. The failure in this specimen was caused by major diagonal shear cracks within the CSS with no sign of debonding as shown in Fig. 28b.

a) G-F-S b) G-I-S

Figure 28: Crack patterns and failure modes for G-FRCM specimens.

4.1.2. Test Results for Hybrid NSE/EB-FRCM

A summary of the experimental test results for the hybrid NSE/EB-FRCM specimens is given in Table 8. Discussion on the results of these specimens in terms of the load carrying capacity and deformational characteristics is provided in this section, while detail discussion on the crack patterns and failure modes is provided in Section 4.3.4.

Table 8

Summary of the Test Result (Hybrid NSE/EB-FRCM)

1	2	3	4	5	6	7	8
Specimen ID	P_u (kN)	Gain in P_u (%)	δ_u (mm)	Ψ (kN.mm)	$\varepsilon_{s,u}$ ($\mu\varepsilon$)	$\varepsilon_{c,u}$ ($\mu\varepsilon$)	$\varepsilon_{FRCM,u}$ ($\mu\varepsilon$)
R	104	-	3.25	238	1425	-	-
C-F-F	222	114	7.96	1189	-	-	-
C-I-F	206	98	6.21	761	1837	1615	345
P-F-F	183	76	6.41	760	2471	1779	166
P-I-F	170	63	6.30	653	1884	1329	348
G-F-F	187	80	7.44	932	2565	1581	1840
G-I-F	185	78	6.24	717	2057	1251	387

Specimen C-F-F showed an ultimate load of 222 kN corresponding to 114% gain in P_u relative to the reference specimen (R). The shear capacity gradually dropped after the peak load. The maximum deflection of 7.96 mm was observed corresponding to 145% increase relative to R. This specimen showed an energy absorption of 1,189 kN.mm corresponding to 399% enhancement relative to the reference specimen as listed in Column 5 of Table 8. On the other hand, Specimen C-I-F showed an ultimate load value of 206 kN

corresponding to 98% gain in P_u relative to R. This specimen showed 91% higher deflection at P_u and 220% gain in the energy absorption compared to that for Specimen R as listed in Table 8.

Specimen P-F-F failed at an ultimate load of 183 kN corresponding to 76% gain in P_u relative to R. This specimen showed 97% higher deflection at the peak load and 219% gain in the energy absorption compared to that for the Specimen R as listed in Table 8. The gain in P_u for the Specimen P-I-F was 63% relative to R. This specimen exhibited 94% higher deflection at P_u and 174% gain in the energy absorption compared to that for the Specimen R.

Specimen G-F-F showed an ultimate load carrying capacity of 187 kN corresponding to 80% gain relative to R. This specimen exhibited 129% higher deflection at the peak load and 292% gain in energy absorption compared to that for the Specimen R as listed in Table 8. Specimen G-I-F failed at an ultimate load of 185 kN corresponding to 78% gain in P_u relative to R. This specimen exhibited 92% higher deflection at P_u and 201% gain in energy absorption compared to that for the Specimen R.

4.2. Discussion of Test Results (NSE-FRCM)

4.2.1. Ultimate Load Carrying Capacity

As discussed earlier, the ultimate load carrying capacity of each specimen and the percentage of gain in P_u relative to the associated reference specimens are given in the second and third columns of Table 7, respectively. The strengthening system showed significant increase in P_u whith percentage of gain that ranged between 14% and 77% relative to the reference specimens, which indicates a successful application of the NSE-FRCM system for the shear strengthening of RC beams. The effectiveness of the strengthening system varied based on the tested parameters.

4.2.1.1. Fabric Type

Figure 29 shows the effect of the FRCM fabric type on the percentage of gain in the ultimate load carrying capacity. The highest increase in the ultimate load carrying capacity was observed for carbon FRCM strengthened specimen, C-F as shown in Fig. 29 and Table 7. This specimen failed at an ultimate load of 184 kN, which corresponds to 77% increase in P_u relative to R as listed in Table 7. The PBO- and G-FRCM counterparts of the same specimen failed at the ultimate loads of 169 kN and 174 kN, respectively as shown in Fig. 29. These P_u values correspond to 63% increase for Specimen P-F and 67% increase for Specimen G-F in the ultimate load carrying capacity relative to the reference specimen as listed in Table 7. Similarly, for specimens with TSR within the CSS, C-FRCM performed better than PBO- and G-FRCM counterparts as shown in Fig. 29. For example, the specimen with TSR within the CSS and strengthened with full configuration of C-FRCM system, C-F-S, showed 46% gain in P_u. However, this gain in P_u was reduced to

29% and 38% for PBO-FRCM and G-FRCM counterparts, i.e., P-F-S and G-F-S, respectively as shown in Fig. 29 and Table 7. In all other cases, C-FRCM strengthened specimens performed better than that of the PBO- and G-FRCM counterparts as shown in Fig. 29. Moreover, with an exception of Specimen G-I, G-FRCM strengthened specimens showed higher enhancement in the ultimate load carrying capacity than that for the PBO-FRCM counterparts as shown in Fig. 29. Specimen G-I showed 34% gain in the ultimate load carrying capacity, which was lower than that of PBO-FRCM counterpart, P-I (47%) as listed in Table 7.

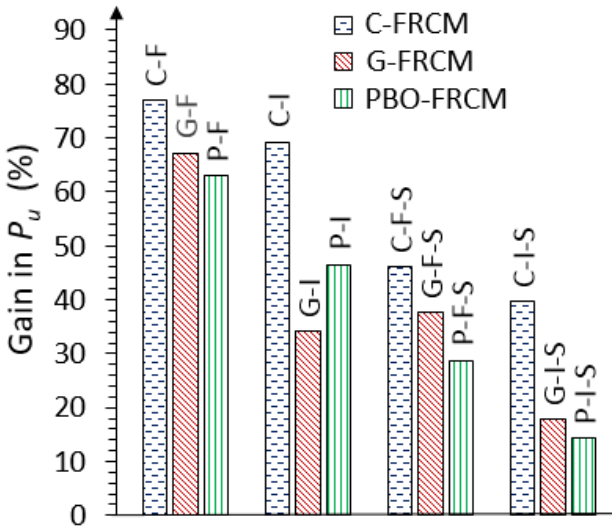

Figure 29: Effect of FRCM type on the gain in the ultimate load carrying capacity.

4.2.1.2. FRCM Configuration

Figure 30 shows the effect of FRCM configuration on the percentage of gain in the ultimate load carrying capacity. The full FRCM configuration behaved better than the intermittent counterpart in terms of the increase in P_u as shown in Fig. 30. For instance, full configuration for PBO-FRCM, P-F (63%), showed 16% higher enhancement in P_u than that of its intermittent counterpart, P-I (47%) as shown in Fig. 30. The difference was more pronounced in the case of G-FRCM strengthened beams in which specimens strengthened with full configuration in Specimens G-F (67%) and G-F-S (38%) showed almost double the enhancement in P_u (67%) that of their intermittent counterparts, G-I (34%) and G-I-S (18%), as shown in Fig. 30 and Table 7. Similar trend was observed for specimens with TSR within the CSS. The maximum enhancement in the load carrying capacity for the specimens with TSR within the CSS was recorded for Specimen C-F-S (46%) as shown in Fig. 30. Changing the FRCM configuration of this specimen to intermittent strips, C-I-S, reduced the gain in the ultimate load carrying capacity to 40%. Moreover, full configuration of both G-FRCM and PBO-FRCM system, G-F-S (38%) and P-F-S (29%), showed higher enhancement in the ultimate load carrying capacity compared to that for their intermittent strips as shown in Fig. 30.

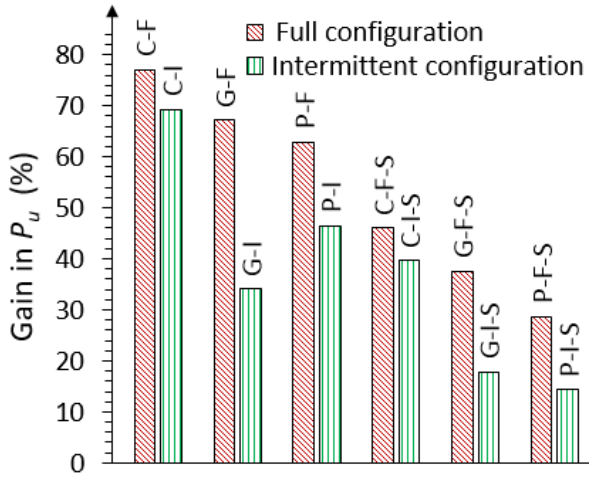

Figure 30: Effect of FRCM configuration on the gain in the ultimate load carrying capacity.

4.2.1.3. FRCM/TSR Interaction Effect on the Ultimate Load Carrying Capacity

Figure 31 shows the effect of the presence of TSR within the CSS on the performance of FRCM system. The efficacy of the FRCM system was reduced by the provision of TSR within the CSS as shown in Fig. 31. For instance, the maximum enhancement in the ultimate load carrying capacity of 77.1% was observed in Specimen C-F, without TSR. This gain in P_u was reduced to 46.0% in Specimen C-F-S, with TSR, as shown in Fig. 31 and Table 7. Moreover, an overall average gain in the ultimate load carrying capacity of 59.5% was observed for beams without TSR within the CSS, which was almost double that for beams with TSR (30.7%) owing to the load sharing between the

TSR and FRCM system confirming the FRCM/TSR interaction. Similar results have been reported for externally bonded FRCM [57,77] and FRP [14] systems.

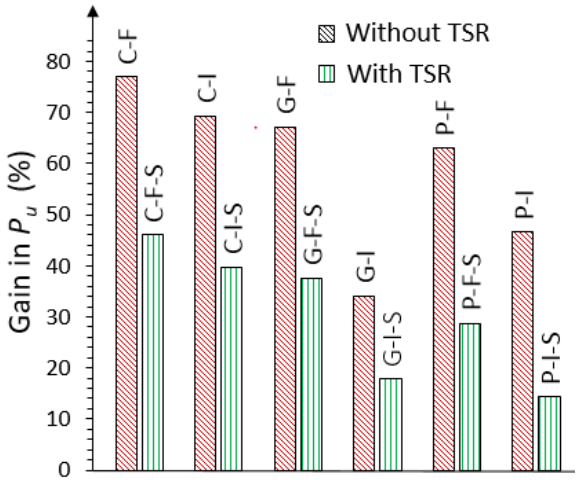

Figure 31: Effect of FRCM/TSR interaction on the gain in the ultimate load carrying capacity.

4.2.2. Load–deflection Response

Figures 32 and 33 show the load–deflection plots for the beams without TSR within the CSS and with TSR, respectively. Moreover, the fourth column of Table 7 lists the deflection at P_u (δ_u). The FRCM strengthening system has significantly increased the deflection of the strengthened beams relative to the associated reference specimens as shown in Figs. 32 and 33 and Table 7. Figure 34 shows the effect of FRCM/TSR

interaction on the percentage increase in δ_u. The presence of TSR within the CSS reduced the percentage of increase in the deflection at P_u relative to the associated reference beam as shown in Fig. 34. For the beams without TSR within the CSS, the increase in the deflection at P_u ranged from 35.4% to 99.4% relative to the associated reference beam (R = 3.25 mm), while for the beams with TSR it ranged from 26.9% to 85.9% relative to the associated reference beam (R-S = 4.69 mm), as given in Table 7. Generally, C-FRCM beams experienced higher deflection at the ultimate load compared to those for G-FRCM beams, which was in turn higher than those of PBO-FRCM beams as shown in Figs. 32 and 32. As for the FRCM configuration, the beams strengthened with full FRCM configuration showed higher increase in the deflection at P_u than those of the intermittent configuration counterparts.

As can be seen in Figs. 32 and 33, the strengthened beams experienced different post-peak kinds of behavior. The beams with TSR within the CSS experienced a more ductile behavior as compared to those of the TSR free counterparts as seen in Figs. 32 and 33. Generally, carbon FRCM and glass FRCM strengthened beams exhibited relatively softer post-peak behavior compared to those of PBO-FRCM counterparts.

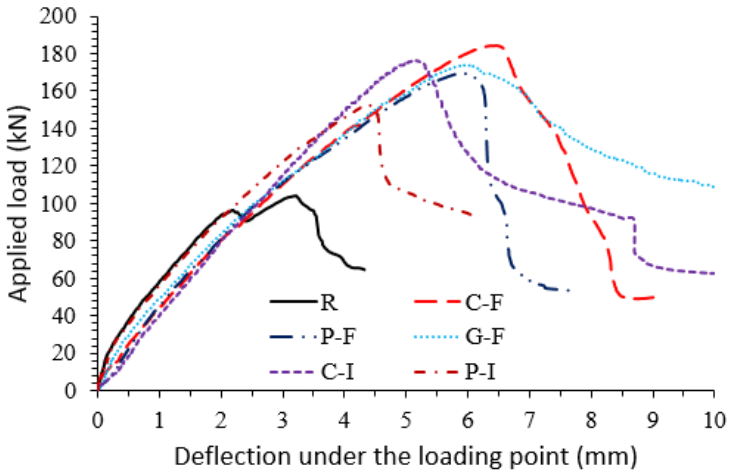

Figure 32: Applied load versus deflection plots for beams without TSR within the CSS.

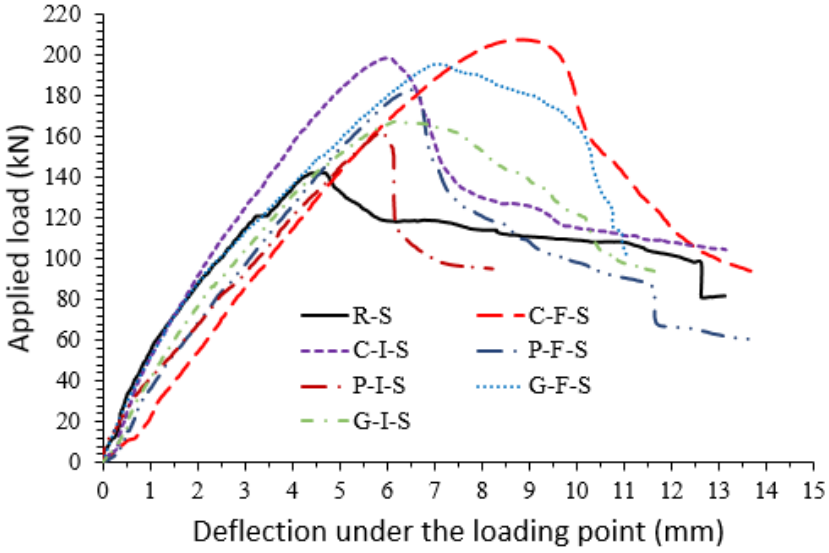

Figure 33: Applied load versus deflection plots for beams with TSR within the CSS.

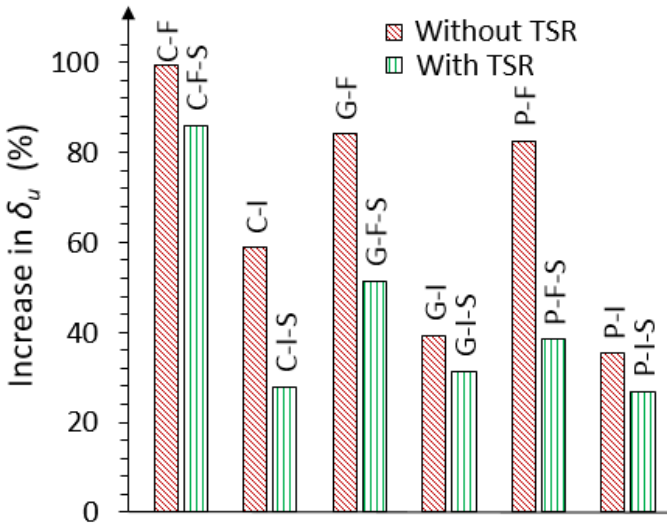

Figure 34: Effect of the FRCM/TSR interaction on the percentage increase in the deflection at P_u.

4.2.3. Energy Absorption

Energy absorption (Ψ) is the area under the load–deflection curve up to the peak load [48]. The strengthening system has enhanced the energy absorption of the strengthened beams as listed in the fifth column of Table 7. Figure 35 shows the effect of the FRCM/TSR interaction on the percentage of gain in Ψ. The TSR within the CSS resulted in a lower increase in the energy absorption compared to that for the beams without TSR as shown in Fig. 35. An average overall gain of the energy absorption for the beams without TSR was 143.0%, relative to the associated reference beam (R), which was more than twice that for the beams with TSR within the CSS (67.0% relative to R-S).

Generally, carbon FRCM was the most effective of all the systems in terms of the increase in the energy absorption. For instance, Specimen C-F showed Ψ value of 753 kN.mm corresponding to 216% increase in Ψ which was higher than the values for its glass and PBO-FRCM counterparts, i.e., G-F (192%) and P-F (166%) as listed in Table 7. Furthermore, full FRCM configuration showed better performance than that of the intermittent counterpart in increasing the absorption energy of the strengthened beams. This observation confirmed the importance of the quantity of FRCM within the CSS.

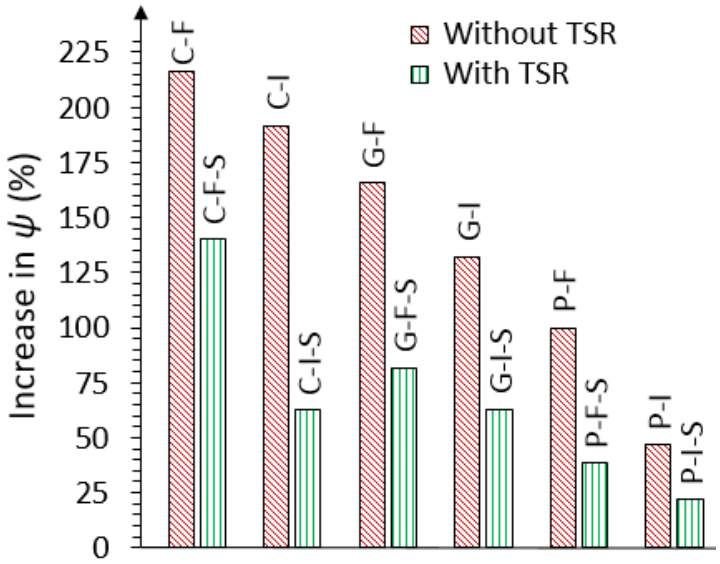

Figure 35: Effect of the FRCM/TSR interaction on the percentage increase in the energy absorption.

4.2.4. Crack Propagation and Failure Modes

As discussed earlier, all specimens exhibited a shear failure mode caused by the propagation of shear cracks within the CSS. In all strengthened beams except C-F, which failed in FRCM/concrete debonding, the failure was governed by fabric rupture with no signs of FRCM/concrete debonding or delamination within the FRCM system. This observation illustrates that the NSE strengthening system can significantly enhance the FRCM/concrete interaction and thus mitigate the debonding failure commonly observed in the conventional externally bonded FRCM system. The beams strengthened with continuous FRCM system failed through the formation of multiple diagonal cracks within the CSS. However, a wider single diagonal crack has been observed for beams strengthened with intermittent FRCM configuration.

4.2.5. Analysis of Crack Width

The plots for the crack width versus the load are shown in Figs. 36 through 38. As can be seen in Figs. 36 and 37, the beams with TSR within the CSS showed smaller crack widths compared to those for the beams without TSR due to the increased aggregate interlock provided by the presence of the TSR [14,78]. For instance, the crack width for Specimen P-I was 1.37 mm at the ultimate load of 152 kN. At this load, Specimen P-I-S, with TSR within the CSS, showed a smaller crack width of 0.62 mm as shown in Fig. 37.

From Figs. 36 through 38, it is evident that the FRCM strengthening system has significantly reduced the crack width of the strengthened beams relative to the associated reference beams. For instance, for beams without TSR within the CSS, the crack width of 0.81 mm was measured for the reference beam (R) at the ultimate load of 104 kN. At the

same load, the crack widths measured for Specimens C-F, P-F, P-I, G-F, and G-I were 0.09 mm, 0.22 mm, 0.33 mm, 0.17 mm, and 0.37 mm, respectively (as can be seen in Fig. 38).

Regarding the FRCM type, C-FRCM beams showed smaller crack widths compared to those of PBO-FRCM beams as the former utilize the fibers in both the weft and warp directions almost equally. Furthermore, full configuration led to lower crack width values compared to that of the intermittent counterpart as shown in Figs. 36 through 38.

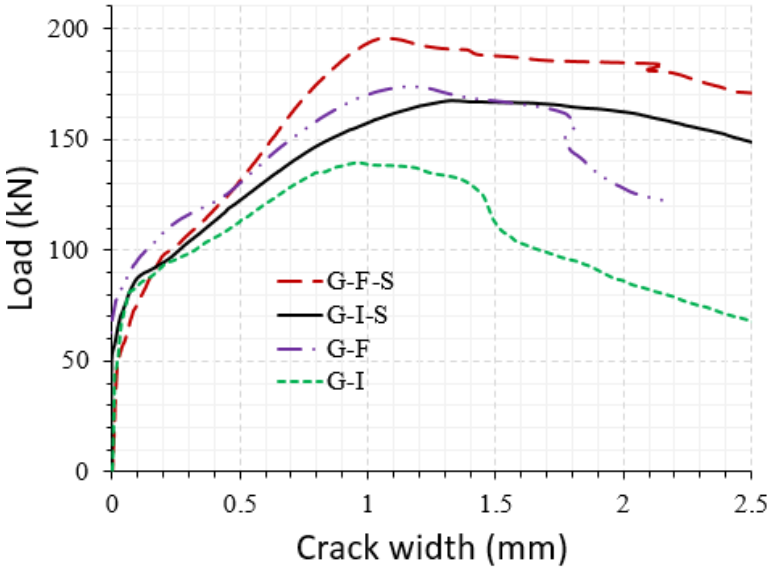

Figure 36: Load versus crack width plots for G-FRCM beams.

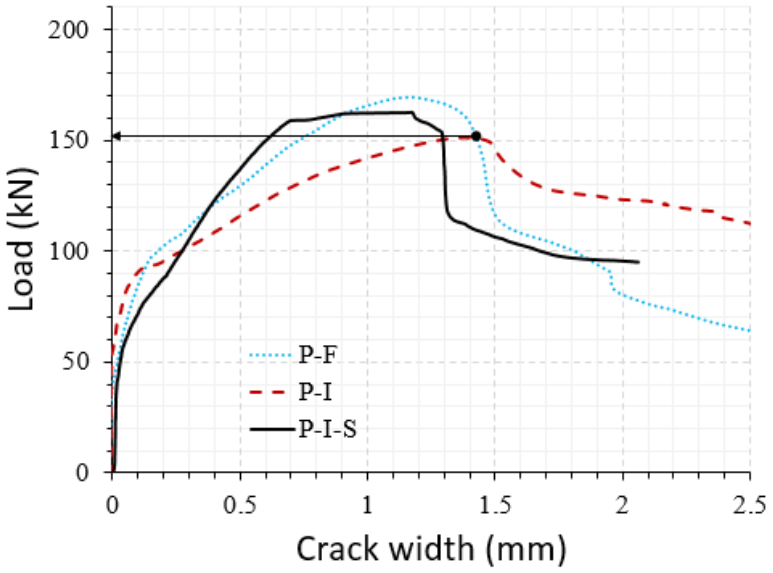

Figure 37: Load versus crack width plots for PBO-FRCM beams.

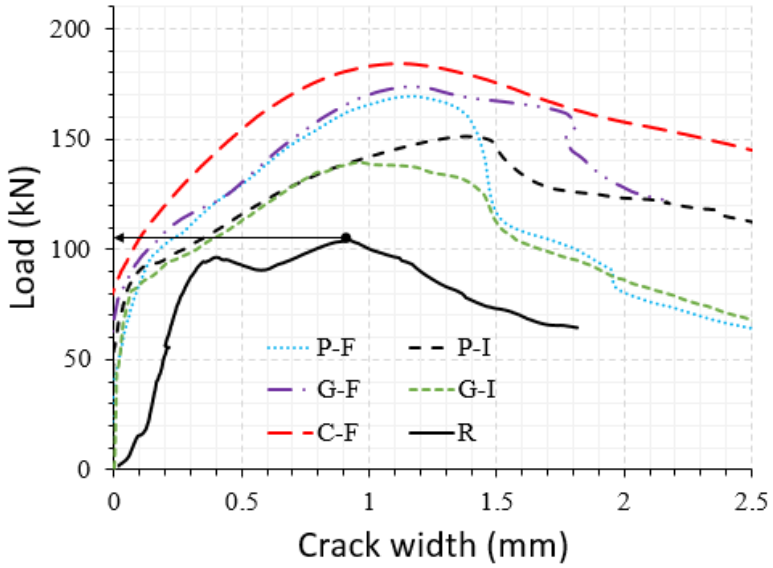

Figure 38: Load versus crack width plots for beams without TSR within the CSS.

4.2.6. Steel Reinforcement and Concrete Strains

The strain in the tensile reinforcement bars at the ultimate load, $\varepsilon_{s,u}$, is listed in the sixth column of Table 7. The tensile steel strains at P_u for the reference beams R and R-S were 1425 με and 2000 με, respectively. With an exception of C-FRCM, the provision of TSR within the CSS lowered the percentage increase in $\varepsilon_{s,u}$ with respect to the associated reference specimens. For instance, the strains in the flexural reinforcement at the ultimate load for Specimens G-F and P-F was almost 70% higher than that of the reference specimen. However, Specimens G-F-S and P-F-S showed an increase in $\varepsilon_{s,u}$ of about 40% higher than that of R-S.

The strengthening system has significantly increased the strains in the longitudinal bars, which indicated that it is effective in delaying the brittle shear failure. Generally, carbon FRCM strengthened beams showed higher flexural strains than those of the PBO and glass FRCM strengthened beams with an exception of Specimen C-I. With regard to the FRCM configuration, full strengthening configuration showed higher tensile strains than that shown by the intermittent counterparts. For instance, Specimens C-F and G-F-S showed respective tensile strains of 2711 με and 2768 με that were higher than the values observed for their intermittent counterparts, i.e., C-I (1787 με) and G-I-S (2137 με), respectively (as listed in Table 7).

The concrete strains measured at the ultimate load ($\varepsilon_{c,u}$) were below that at the crushing point (3500 με) confirming brittle failure as listed in Table 7. Generally, carbon FRCM beams exhibited higher compressive concrete strains compared to those of glass and PBO-FRCM counterparts. Moreover, the concrete strains in full FRCM strengthened

beams were generally higher than those of the intermittent FRCM counterparts as listed in Table 7.

4.2.7. TSR and FRCM Strains

The maximum strains in the TSR within the CSS was recorded. Figures 39a through 39c showed the load versus TSR strains plots for C-, PBO- and G-FRCM strengthened beams, respectively. As can be seen in these figures, the strengthened beams exhibited lower strains in the TSR compared to that of the reference beam (R-S) due to the load sharing between the TSR and the FRCM system. For instance, the strains developed in the reference beam (R-S) at the ultimate load of 142 kN was 2500 με. At the same load, Specimens C-F-S and C-I-S exhibited respective strains of 238 με and 1540 με in the TSR as shown in Fig. 39a. This result confirmed the FRCM/TSR interaction, which was reported for externally bonded FRCM [57,77] and FRP [14] systems. Moreover, full configuration of FRCM system led to further reduction in the TSR strains compared to those of the intermittent configuration.

For the intermittent configuration, the strains in the FRCM composites were generally higher in the middle strips than those for the outer strips as the shear cracks occurred mostly at the middle strip location. The maximum strains in the FRCM at the ultimate load are listed in the last column of Table 7. In some of the beams, the major shear crack did not intersect with the FRCM strain gauge locations that resulted in very low strains recorded for FRCM. Full FRCM configuration led to higher strains in the FRCM indicating better utilization of the strengthening composite in the full FRCM configuration as listed in Table 7.

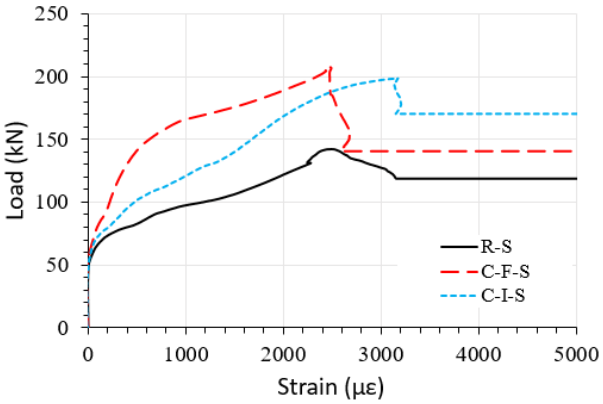

(a)

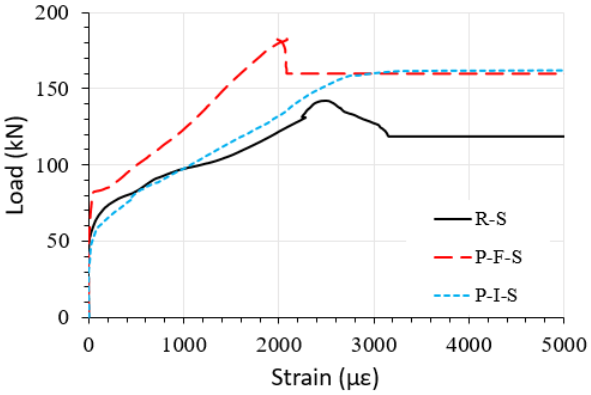

(b)

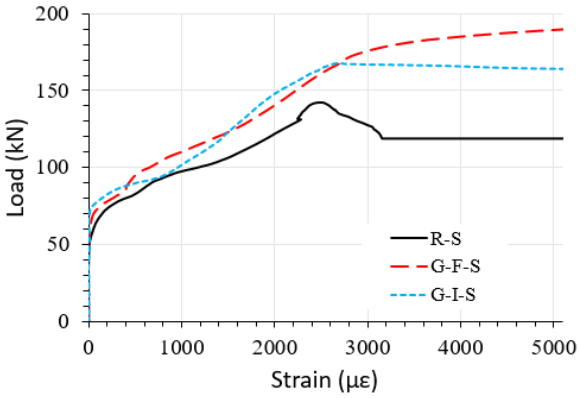

(c)

Figure 39: Load versus TSR strains plots for specimens strengthened with (a) carbon FRCM, (b) PBO–FRCM, and (c) glass FRCM.

4.3. Discussion of Test Results (Hybrid NSE/EB-FRCM)

4.3.1. Ultimate Load Carrying Capacity

As discussed earlier, the second and third columns of Table 8 provide the ultimate load carrying capacity (P_u) and the gain in P_u, respectively. The average overall gain in the ultimate load carrying capacity was 85% that demonstrates a successful application of the hybrid NSE/EB-FRCM strengthening system for shear critical RC beams.

Figure 40 shows the effect of FRCM type on the percentage of gain in the ultimate load carrying capacity. Similar to the NSE-FRCM system, C-FRCM showed higher enhancement in P_u than that of PBO- and G-FRCM counterparts as shown in Fig. 40. The highest gain in P_u was recorded for Specimen C-F-F (114%) as shown in Fig. 40 and Table 8. The G- and PBO-FRCM counterparts of the same configuration, G-F-F and P-F-F, showed 80% and 76% gain in P_u, respectively as shown in Fig. 40 and Table 8.

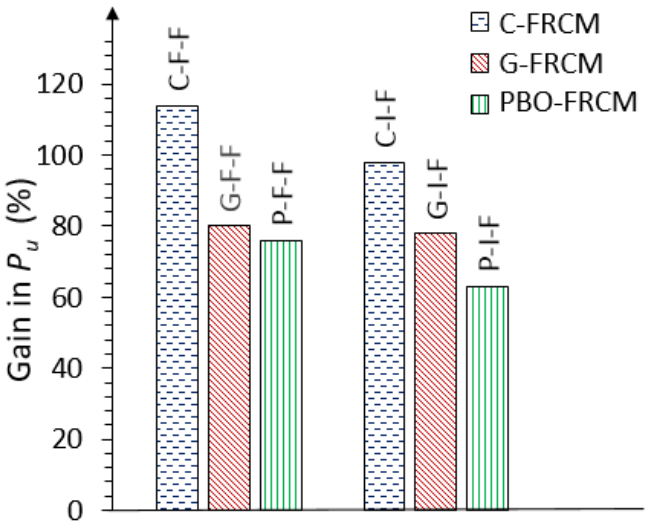

Figure 40: Effect of FRCM type on the percentage of gain in the ultimate load carrying capacity.

Figure 41 shows the effect of FRCM configuration on the percentage of gain in the ultimate load carrying capacity. Full FRCM configuration for both NSE and EB part showed better performance than those involving intermittent configuration as shown in Fig. 41. For instance, Specimen P-F-F failed at an ultimate load of 183 kN which yields 76% gain in P_u. Replacing full configuration of near surface embedded part with intermittent strips in Specimen P-I-F lowered the gain in P_u to 63% as shown in Fig. 41 and Table 8.

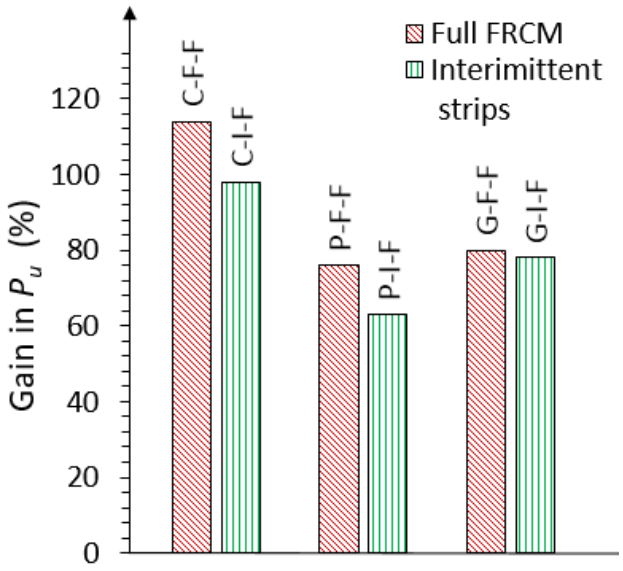

Figure 41: Effect of FRCM configuration on the percentage of gain in the ultimate load carrying capacity.

Figure 42 shows the effect of the additional two layers of EB-FRCM on the percentage gain in the ultimate load carrying capacity. The addition of two layers of EB-FRCM system increased the ultimate load carrying capacity of the strengthened specimen compared to those of the specimens strengthened with only two layers of NSE-FRCM system of the same configuration as shown in Fig. 42. Specimen C-F-F, with four layers of FRCM, reached a higher load of 222 kN compared with that for the Specimen C-F (184 kN) owing to the contribution of the additional two layers of EB-FRCM as shown in Fig. 42. In PBO- and G-FRCM, specimens strengthened with four layers of FRCM, P-F-F (76%) and G-F-F (80%), showed higher gain in the ultimate load carrying capacity

compared with their two layers counterparts, P-F (63%) and G-F (67%) as shown in Fig. 42. However, the gain in P_u was not proportional to the number of FRCM layers owing to the initiation of the debonding failure caused by the additional two layers of EB-FRCM system.

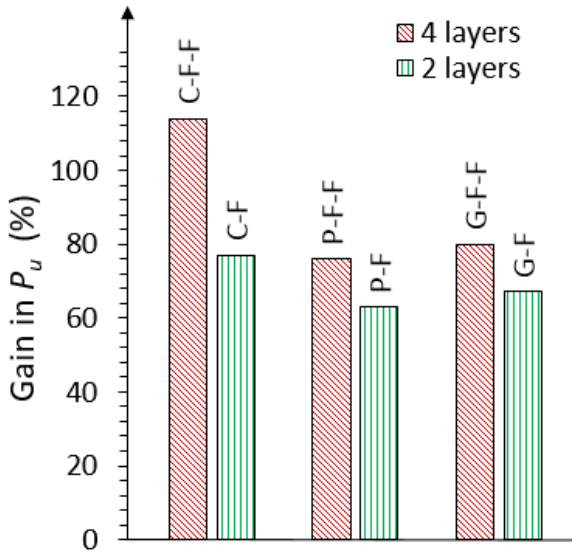

Figure 42: Effect of additional two layers of EB-FRCM on the percentage of gain in the ultimate load carrying capacity.

4.3.2. Load–deflection Response

The effect of the strengthening configuration on the load versus displacement plots are shown in Fig. 43 through Fig. 45 for carbon FRCM, PBO-FRCM, and glass FRCM

strengthened specimens, respectively. From these figures, it can be seen that no yield zone has been observed in all specimens indicating that the steel reinforcement did not reach the yielding point. This result confirmed the shear failure in all specimens provided that the concrete in the compression zone did not crush.

As shown in Fig. 43 through Fig. 45, different kinds of post-peak behavior have been observed for the strengthened specimens. Specimen P-I-F strengthened with full configuration of EB and intermittent strips of near surface embedded PBO-FRCM, as an example, showed softening behavior during the post-peak zone representing traces of resistance attributed to the strengthening system.

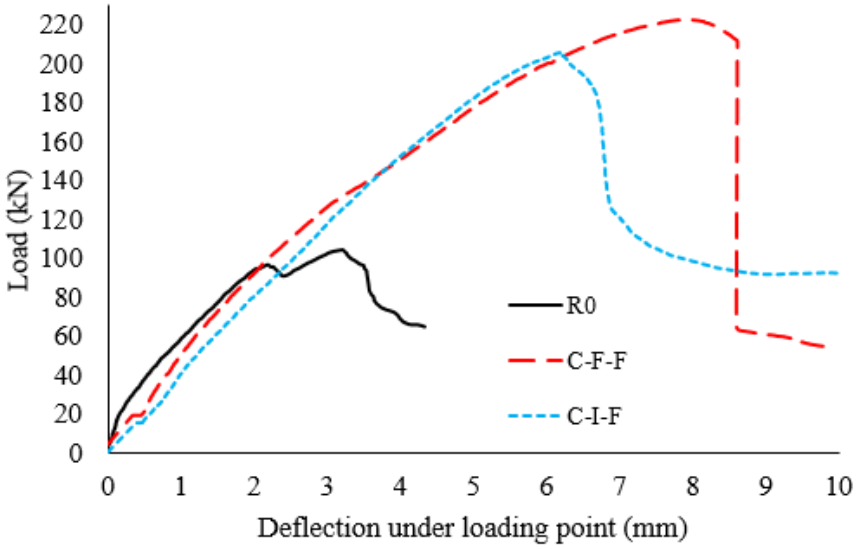

Figure 43: Effect of the strengthening configuration on the load versus displacement plots for carbon FRCM.

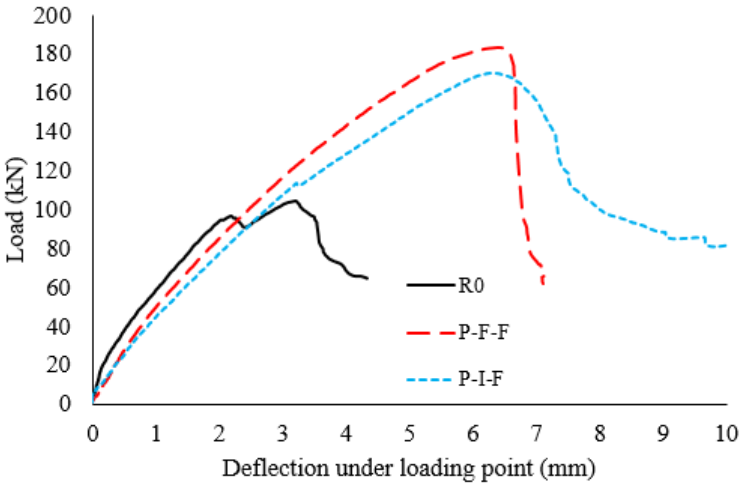

Figure 44: Effect of the strengthening configuration on the load versus displacement plots for PBO-FRCM.

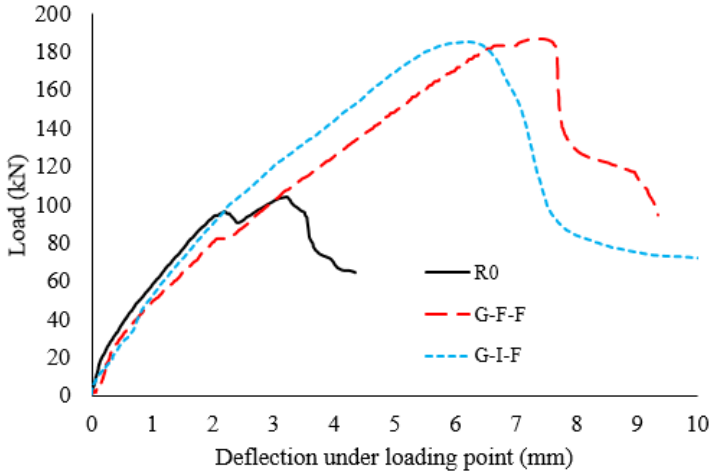

Figure 45: Effect of the strengthening configuration on the load versus displacement plots for glass FRCM.

The deflection at the peak load, δ_u, for all specimens is listed in the fourth column of Table 8. The strengthening system resulted in higher values of δ_u relative to that for the reference specimen. An average of 108% increase in δ_u was observed relative to the reference specimen (R = 3.25 mm). Full FRCM configuration showed higher deflection at the peak load compared to that for the intermittent configuration counterparts. For instance, specimen strengthened with full configuration of glass FRCM, G-F-F (7.44 mm), showed higher deflection at the peak load than its intermittent counterpart, G-I-F (6.24 mm) as listed in Table 8.

4.3.3. Energy Absorption

The hybrid NSE/EB-FRCM strengthening has significantly improved the energy absorption of the strengthened specimens a listed in the fifth column of Table 8. The highest enhancement in the energy absorption was observed in Specimen C-F-F (1,189 kN.mm), which was about 5 times that for the reference specimen (R = 238 kN.mm). Glass FRCM and PBO-FRCM counterparts of the same configuration, G-F-F and P-F-F, showed respective energy absorption values of 932 kN.mm and 760 kN.mm as listed in Table 8. In all cases, carbon FRCM specimens showed higher enhancement in the energy absorption compared to that for the glass FRCM counterparts. Moreover, glass FRCM specimens exhibited higher energy absorption values compared to that for the PBO-FRCM counterparts.

The full strengthening configuration exhibited higher increase in the energy absorption than its intermittent counterpart. For instance, Specimen C-F-F (1189 kN.mm)

showed 180% higher enhancement in the energy absorption compared to that for Specimen C-I-F (761 kN.mm) as listed in Table 8.

Provision of an additional two layers of externally bonded FRCM system on the NSE-FRCM significantly increased the energy absorption values compared to those with only two layers of the NSE-FRCM. The Specimens C-F, G-F, and P-F showed respective energy absorption values of 753 kN.mm, 694 kN.mm, and 632 kN.mm, which were lower than that for the hybrid NSE/EB-FRCM counterparts, i.e. C-F-F (1189 kN.mm), G-F-F (932 kN.mm), and P-F-F (760 kN.mm) as listed in Table 7 and Table 8.

4.3.4. Crack Propagation and Failure Modes

As discussed earlier, all specimens failed in shear. The crack patterns and failure modes of each specimen strengthened with hybrid NSE/EB-FRCM technique are shown in Figs. 46a through 46f. Major diagonal shear cracks have been observed on the surface of the FRCM for all specimens involving intermittent configuration as shown in Figs. 46a through 46c for Specimens C-I-F, P-I-F, and G-I-F, respectively. However, the specimens strengthened with full configuration of hybrid NSE/EB-FRCM system did not show a major crack on the surface of the FRCM as seen in Figs. 46d through 46f for Specimens C-F-F, P-F-F, and G-F-F, respectively. Following the completion of the test, the FRCM material was removed to expose the concrete surface to look at the actual crack patterns of the specimens. In fact, after exposing the FRCM layers, it was found that there was always a major diagonal shear crack on the concrete surface for all specimens as shown in Figs. 47a and 47b for Specimen P-F-F before and after removal of the FRCM composite, respectively.

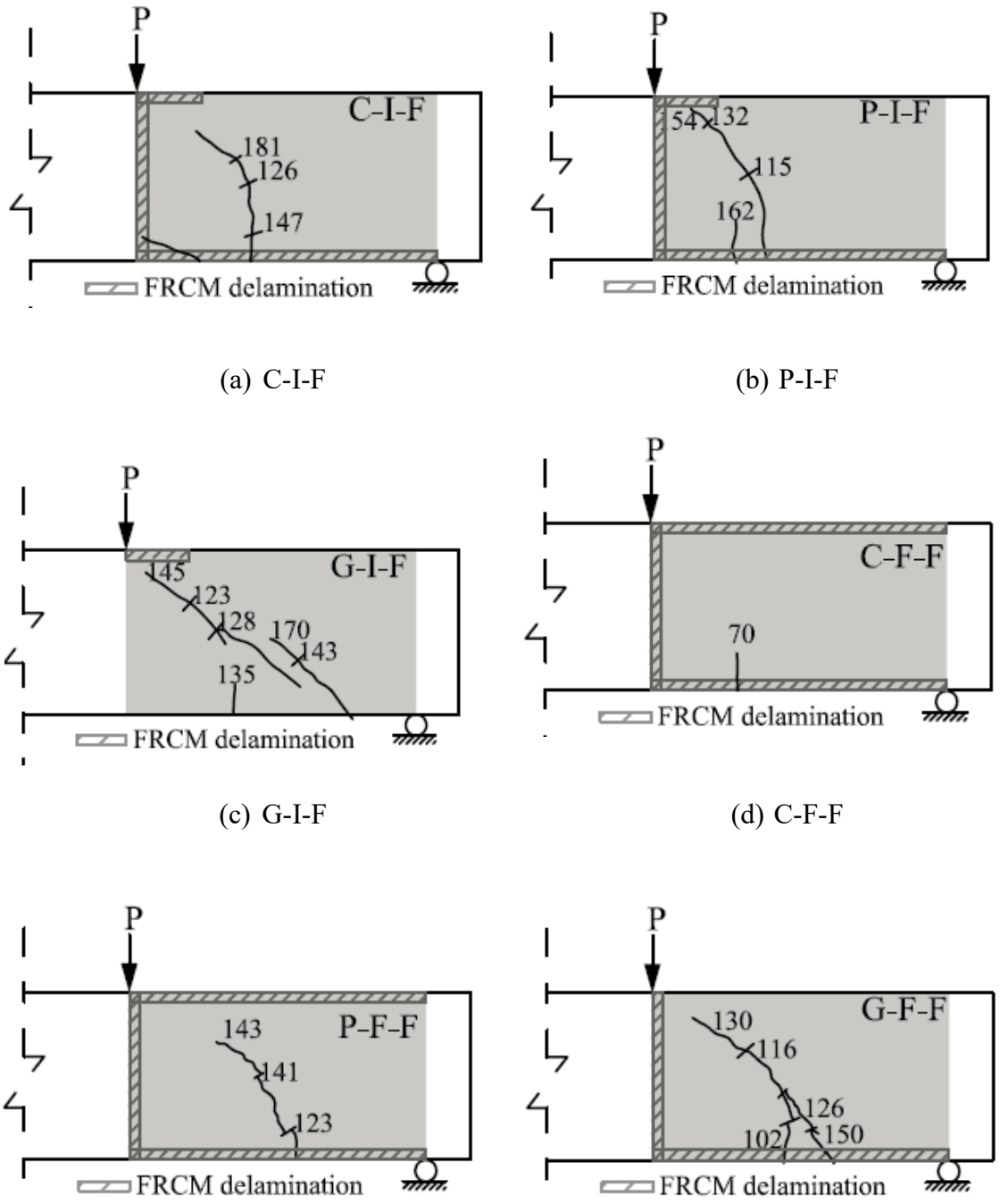

Figure 46: Crack patterns and failure modes for the hybrid NSE/EB-FRCM specimens.

(a) P-F-F (b) P-F-F (FRCM composite removed)

Figure 47: Failure mode of Specimen P-F-F.

The FRCM debonding off the concrete substrate has been observed in all the hybrid NSE/EB-FRCM specimens as shown in Figs. 46a through 46f. Failure in specimens that involved intermittent configuration was characterized by vertical debonding of the first strip directly under the loading point along the beam depth and longitudinal debonding of the FRCM near the bottom of the beam with an exception of specimen G-I-F as shown in Figs. 46a through 46c. In Specimen G-I-F, FRCM debonding was observed only near the top of the beam for the first strip directly under the loading point as shown in Fig. 46c due to the better bond between G-FRCM and concrete substrate.

Full configuration of the hybrid NSE/EB-FRCM system was associated with longitudinal debonding of the FRCM at locations near the bottom and top of the beam with an exception of Specimen G-F-F as shown in Figs. 46d through 46f. For instance, a clear debonding of FRCM off the concrete substrate was observed on top of the beam for Specimen P-F-F as shown in Fig. 47a. In Specimen G-F-F, there was a clear FRCM debonding near the bottom surface of the beam; however, no sign of debonding near the

top of the beam as shown in Fig. 46f owing to the better bond between the G-FRCM and concrete.

4.3.5. Analysis of Crack Width

The available load versus crack width plots at each load step has been provided in Fig. 48. As can be seen in this figure, the crack width of the strengthened specimens has greatly been reduced due to the strengthening system. The crack width at the peak load ($P_u = 104$ kN) for the reference specimen was 0.809 mm. At the same load (104 kN), the crack width measured for Specimens G-F-F and G-I-F were 0.346 mm and 0.145 mm, respectively as shown in Fig. 48.

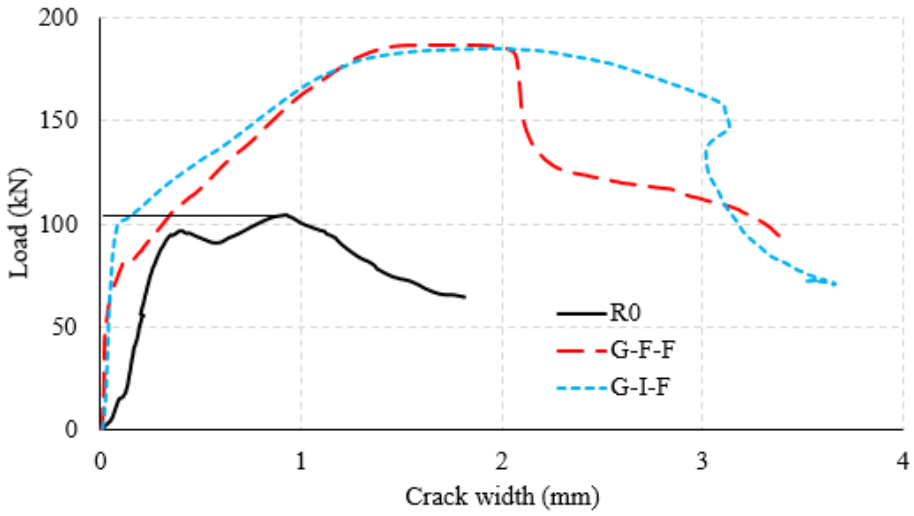

Figure 48: Plots of crack width versus applied load for glass FRCM.

4.3.6. Steel Reinforcement and Concrete Strains

The strains developed in the tensile bar ($\varepsilon_{s,u}$) and compressive strains in concrete ($\varepsilon_{c,u}$) at P_u are listed in Column 6 and Column 7 of Table 8, respectively. Furthermore, the load versus flexural strains diagrams are depicted in Figs. 49 through 51 for G-FRCM, PBO-FRCM and C-FRCM specimens, respectively. The strengthening system has noticeably increased the tensile strains developed in the longitudinal bar with an average increase of 52% as listed in Table 8. The specimen strengthened with full FRCM configuration exhibited higher values of $\varepsilon_{s,u}$ than those involving intermittent configuration. For instance, the value of $\varepsilon_{s,u}$ was higher for Specimen G-F-F (2565με) than that for Specimen G-I-F (2057 με) as listed in Table 8 and Fig. 49. This observation indicates the significance of the FRCM continuity in increasing the tensile strains in the flexural steel bar thereby delaying the brittle shear failure.

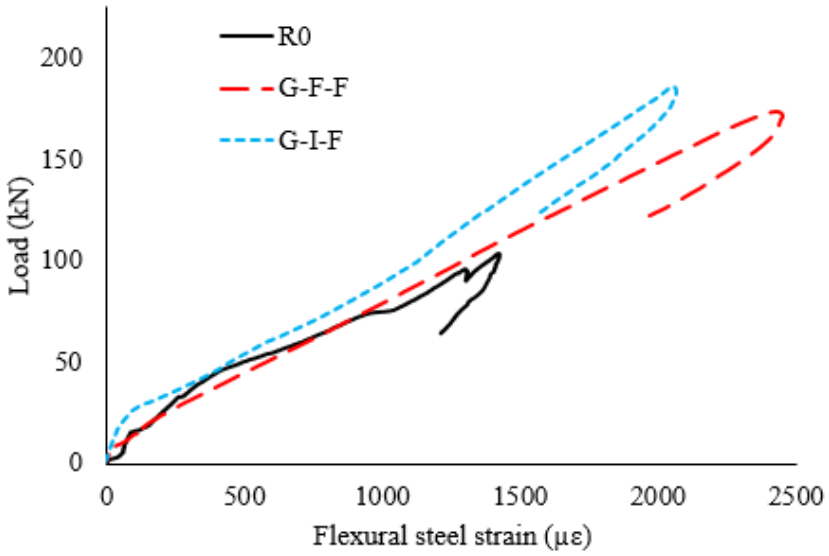

Figure 49: Load–flexural strain diagrams for G-FRCM strengthened specimens.

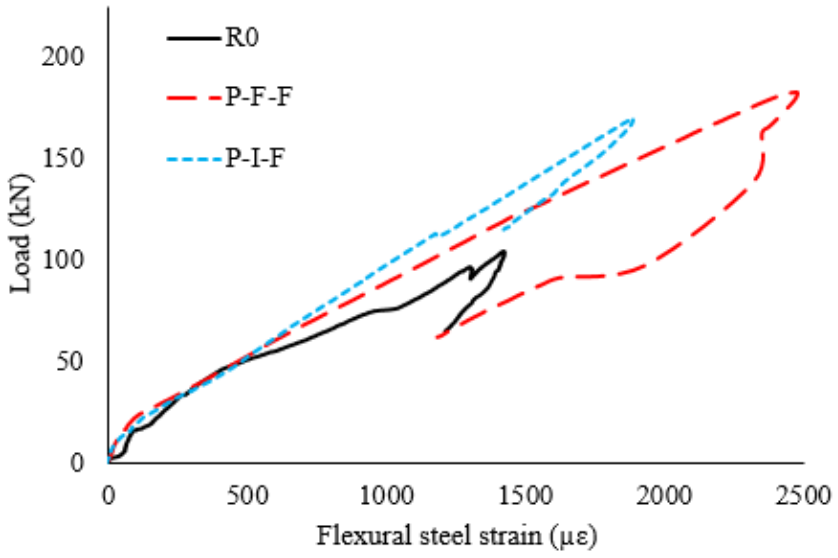

Figure 50: Load–flexural strain diagrams for PBO-FRCM strengthened specimens.

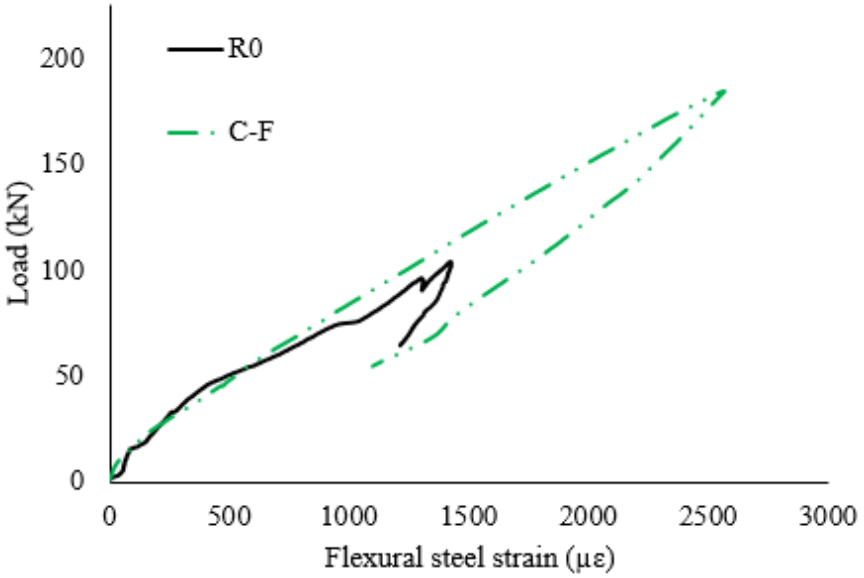

Figure 51: Load–flexural strain diagrams for C-FRCM strengthened specimens.

4.3.7. FRCM Strains

The maximum FRCM tensile strains at P_u, $\varepsilon_{FRCM,u}$, are summarized in the last column of Table 8. The $\varepsilon_{FRCM,u}$ values were very low as the major shear crack did not intersect with the strain gauge locations. The G-FRCM strengthened specimens showed higher FRCM strains compared to those of the PBO-FRCM counterparts attributed to better FRCM/concrete bond in the former as listed in Table 8. For instance, the strains in Specimens G-F-F (1840 με) and G-I-F (387 με) were higher than those for PBO-FRCM counterparts; namely, P-F-F (166 με) and P-I-F (348 με), respectively.

CHAPTER 5: ANALYTICAL FORMULATION

5.1. Introduction

Different models were created to predict the ultimate load carrying capacity of the FRCM strengthened beams in shear revealing different prediction capabilities [44,59,69]. Vecchio and Collins [88] developed a method for predicting the shear capacity of RC beams, i.e., the modified compression field theory (MCFT). This theory accounts for the concrete tensile stresses of the cracked section and requires solving a large number of equations in an iterative process. Bentz et al. [89] developed a simplified version of the MCFT that is referred to as the simplified compression field theory (SCFT) in which the number of parameters and iterations has been reduced. The shear strength of RC elements, in the SCFT, is determined as a function of two parameters; namely, the inclination of the diagonal compressive stress (θ) and the tensile stress factor of the cracked concrete (β). The SCFT will be adopted here to include the effect of the FRCM system.

5.2. Proposed Model

Consider a beam element strengthened with FRCM system in Fig. 52a. The shear in the beam section is resisted by the diagonal tension stress, f_1, and diagonal compression stress, f_2.

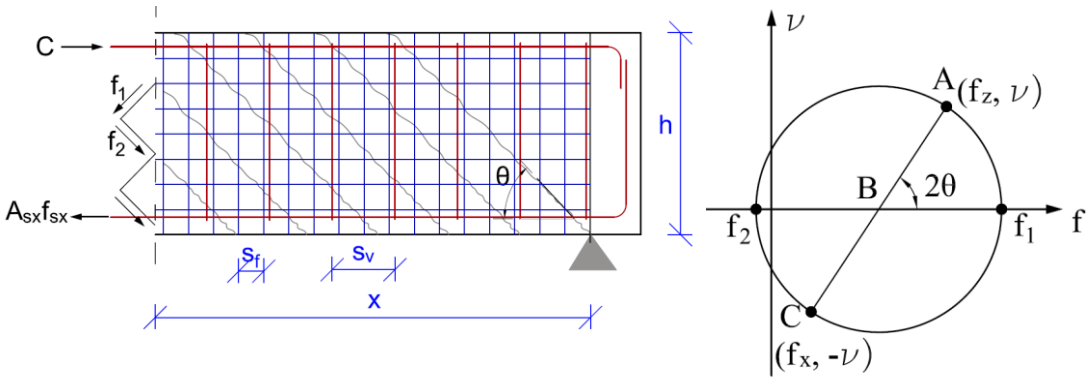

(a) Principal stresses in concrete. (b) Mohr's circle for stresses

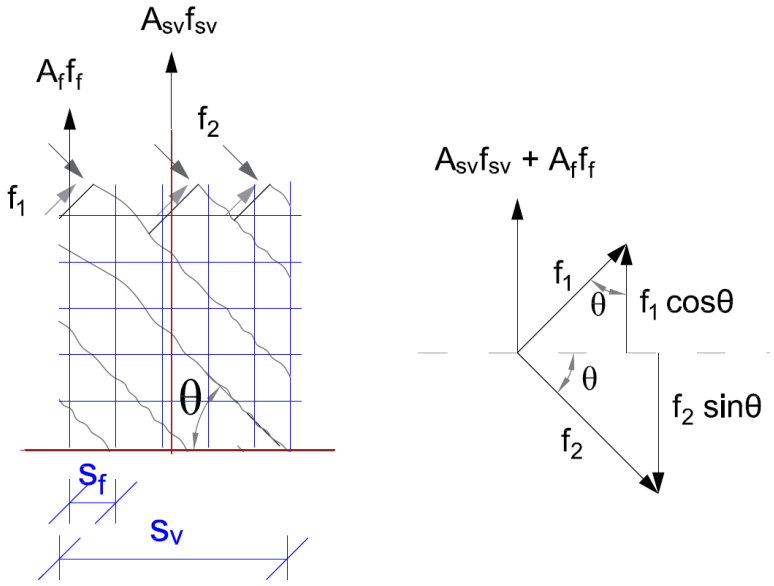

(c) Forces in TSR and FRCM

Figure 52: Equilibrium conditions for the MCFT based on Vecchio and Collins [88].

From the stress equilibrium, as shown in Fig. 52b, the following equation is valid:

$$f_1 + f_2 = \nu\,(\tan\theta + \cot\theta) \quad (1)$$

Where θ is the inclination of the diagonal compressive stress and ν is the shear strength.

From the equilibrium of the forces, Fig. 52c,

$$A_{sv}f_{sv} + A_f f_f = (f_2 \sin^2\theta - f_1 \cos^2\theta)\, b_w S_v \quad (2)$$

Combining Eq. (1) and Eq. (2) and solving for the shear strength,

$$\nu = f_1 \cot\theta + \frac{A_{sv}f_{sv}}{b_w S_v}\cot\theta + \frac{A_f f_f}{b_w S_v}\cot\theta$$

However, $\frac{A_{sv}}{b_w S_v} = \rho_{sv}$ and $\frac{A_f}{S_v} = a_f$.

Thus, the shear strength can be expressed in Eq. (3) below.

$$\nu = f_1 \cot\theta + \rho_{sv}f_{sv}\cot\theta + \frac{a_f}{b_w}f_f \cot\theta \quad (3)$$

Where,

b_w is the width of the web,

A_{sv} and S_v are the area and the spacing of the TSR, respectively,

ρ_{sv} is the reinforcement ratio of the TSR,

f_{sv} is the yield strength of the TSR,

a_f is the area of the fabrics per unit width in the transverse direction, and

f_f is the effective tensile strength of the FRCM.

The effective tensile strength of the FRCM (f_f) can be evaluated by adopting ACI 549 [90] as follows:

$$f_f = \varepsilon_f E_f \quad (4)$$

Where ε_f is the effective tensile strain of the FRCM and E_f is the modulus of elasticity of the FRCM. ACI 549 limits the effective tensile strain of the FRCM, ε_f, to 0.004.

For the strengthening system that involves inclined fabrics at an angle α to the beam length, the shear strength is given by Eq. (5) below.

$$v = f_1 \cot\theta + \rho_{sv} f_{sv} \cot\theta + \frac{a_f}{b_w} f_f \cot\theta \ (\sin\alpha + \cos\alpha) \quad (5)$$

For the intermittent FRCM configuration, the contribution of the FRCM to the shear strength is multiplied by a reduction factor ($R = \frac{N w_s}{L_{CSS}}$), where w_s is the FRCM strip width, L_{CSS} is the critical shear span, and N is the number of FRCM strips. For the full FRCM strengthening configuration $R = 1$.

Thus, the shear strength is given by,

$$v = f_1 \cot\theta + \rho_{sv} f_{sv} \cot\theta + R \frac{a_f}{b_w} f_f \cot\theta \ (\sin\alpha + \cos\alpha)$$

$$v = f_1 \cot\theta + \rho_{sv} f_{sv} \cot\theta + \rho_f f_f \cot\theta \ (\sin\alpha + \cos\alpha)$$

$$v = f_1 \cot\theta + \rho_{sv} f_{sv} \cot\theta + \rho_f \varepsilon_f E_f \cot\theta \ (\sin\alpha + \cos\alpha)$$

$$v = f_1 \cot\theta + \rho_{sv} f_{sv} \cot\theta + \varepsilon_f K_f \cot\theta \ (\sin\alpha + \cos\alpha) \quad (6)$$

Where ρ_f and K_f are the reinforcement ratio and axial rigidity of the FRCM given by equations below,

$$\rho_f = R \frac{a_f}{b_w}$$

$$K_f = \rho_f E_f$$

Therefore, the shear strength is given by Eq. (7) below,

$$v = v_c + v_S + v_f \quad (7)$$

Where ν_c, ν_S and ν_f are the concrete, TSR and FRCM contributions to the shear strength, respectively.

In the SCFT the contribution of the concrete to the shear strength is determined as a function of β, Eq. (8) below.

$$\nu_C = \beta \sqrt{f_c'} \tag{8}$$

Where β is the tensile stress factor given by Eq. (9) below,

$$\beta = \frac{0.4}{1 + 1500\ \varepsilon_x} \frac{1300}{1000 + S_{xe}} \tag{9}$$

Where S_{xe} is the crack spacing given by Eq. (10),

$$S_{xe} = \frac{35 S_x}{a_g + 16} \geq 0.85 S_x \tag{10}$$

Where S_x is the vertical distance between the longitudinal reinforcement (in mm) and a_g is the maximum aggregate size (in mm).

Based on the SCFT, the value of θ is approximated as follows.

$$\theta = (29 + 7000\ \varepsilon_x) \times \left(0.88 + \frac{S_{xe}}{2500}\right) \leq 75° \tag{11}$$

Where ε_x is the strain in the longitudinal reinforcement given by Eq. (12),

$$\varepsilon_x = \frac{\nu \cot\theta - \beta \sqrt{f_c'}\ \tan\theta}{E_s\ \rho_{sx}} \tag{12}$$

Where E_s and ρ_{sx} are the elastic modulus and reinforcement ratio of flexural tensile bars, respectively.

Short beams, with the shear span to effective depth ratio ($x = L_{CSS}/d$) of less than 2.5, exhibit higher shear strength than those of long slender beams as per the ACI-ASCE

Committee 445 [91]. To account for this effect, the contribution of concrete and ITSR to the shear strength is modified as shown in Eq. (13). However, the contribution of FRCM to the shear strength is not affected by the shear span to effective depth ratio as reported in [92].

$$v = K_{sd}\, v_c \; + \frac{x}{2.5K_{sd}} v_S + \; v_f \tag{13}$$

Where K_{sd} is the factor that accounts for the deep beam effect and can be given by Eq. (14).

$$K_{sd} = 1 + \left(\frac{K_b}{x}\right)^{0.6} \tag{14}$$

Where K_b is the boundary of the deep and slender beams, which is considered to be $K_b = 2.5$ as per [91]. For this study, the shear span to effective depth ratio $x = 1.96$.

The proposed model followed the procedure outlined in the flowchart in Fig. 53.

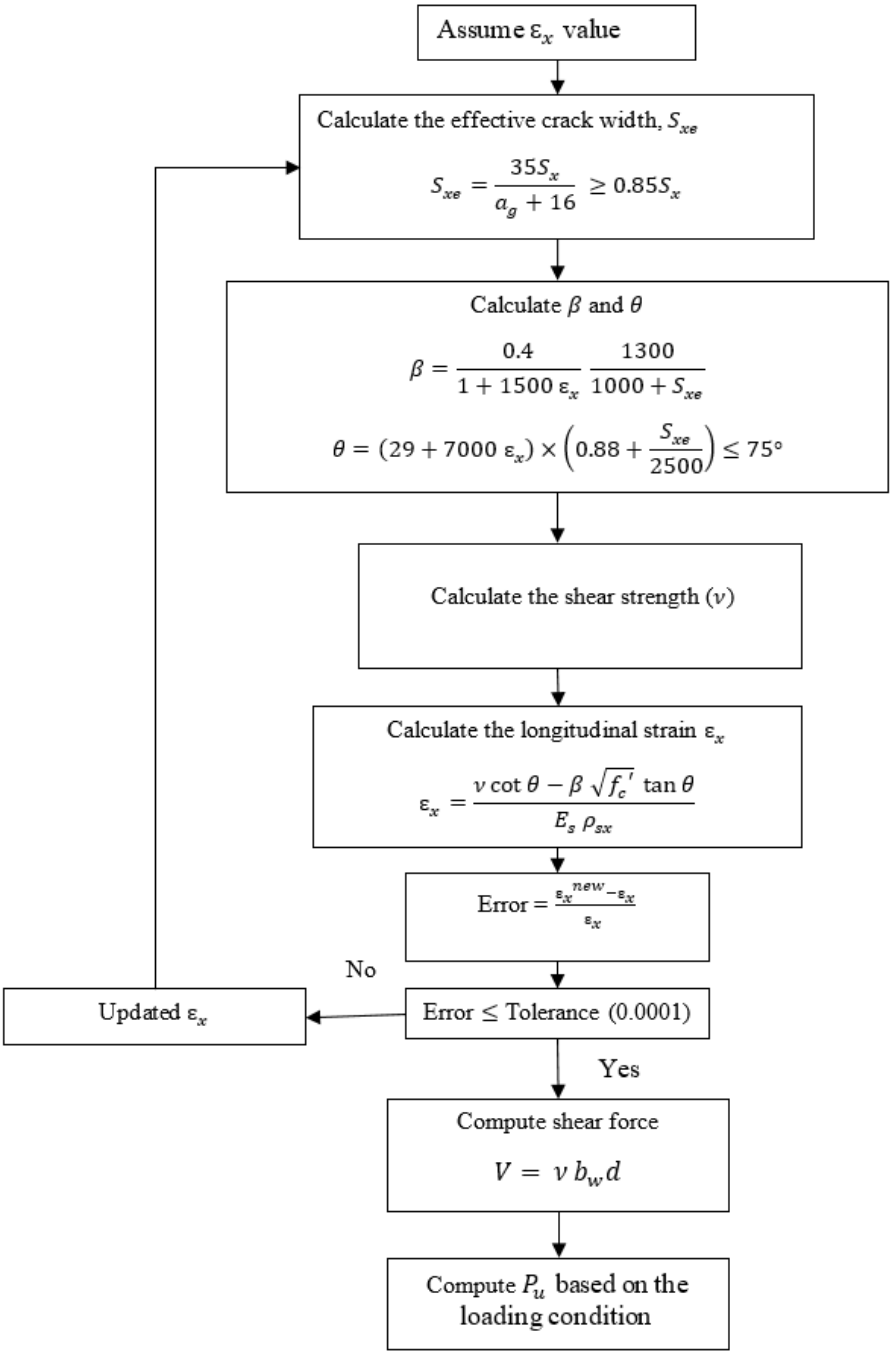

Figure 53: Flowchart for determining the ultimate load carrying capacity of FRCM strengthened beams based on the SCFT.

5.3. Verification of the Proposed Model

Table 9 summarizes the shear strength (v), theoretically predicted ultimate load carrying capacity ($P_{u,th}$) and the ratio of $P_{u,th}$ to experimentally measured ultimate load carrying capacity ($P_{u,ex}$) for the tested beams. The average predicted to experimental ultimate load carrying capacity ($P_{u,th}/P_{u,ex}$) is 94% with a standard deviation of 8%. Moreover, the ultimate load carrying capacity of 62 RC beams, strengthened in shear using different types of FRCM system including carbon (C) FRCM, glass (G) FRCM, basalt (B) FRCM, and PBO-FRCM has been predicted and the results are compared with the experimental results reported in the literature [3,4,47,52,59,69,77,92]. Figure 54 shows the plot for the ratio of the theoretically predicted to the experimental values of the ultimate load carrying capacity. Moreover, the details of the experimental results and the theoretically predicted values of the ultimate load carrying capacity of the beams is summarized in Table 10. As can be seen in Figure 54 and the last column of Table 10, the $P_{u,th}/P_{u,ex}$ ratio ranged between 0.67 and 1.40, while the average of this ratio was 1.04 with a standard deviation of 17%. The results showed that the model can reasonably predict the ultimate load carrying capacity of the strengthened beams.

Table 9

Summary of the Theoretical and Experimental Results (NSE-FRCM Specimens)

Beam	ρ_{sx}	ρ_{sv}	ρ_f	ν (MPa)	$P_{u,th}$ (kN)	$P_{u,ex}$ (kN)	$P_{u,th}/P_{u,ex}$
R	0.0144	-	-	2.1732	128	104.00	1.24
C-F	0.0144	-	0.001253	2.8063	166	184.22	0.90
C-I	0.0144	-	0.000820	2.5867	153	176.08	0.87
G-F	0.0144	-	0.001253	2.4533	145	173.83	0.83
G-I	0.0144	-	0.000820	2.3562	139	139.44	1.00
P-F	0.0144	-	0.001213	2.6812	158	169.46	0.94
P-I	0.0144	-	0.000794	2.5049	148	152.39	0.97
R-S	0.0144	0.0018	-	2.5008	148	142.13	1.04
C-F-S	0.0144	0.0018	0.001253	3.1352	185	207.57	0.89
C-I-S	0.0144	0.0018	0.000820	2.9167	172	198.53	0.87
G-F-S	0.0144	0.0018	0.001253	2.7833	165	195.52	0.84
G-I-S	0.0144	0.0018	0.000820	2.6857	159	167.41	0.95
P-F-S	0.0144	0.0018	0.001213	3.0109	178	182.92	0.97
P-I-S	0.0144	0.0018	0.000794	2.8350	168	162.48	1.03

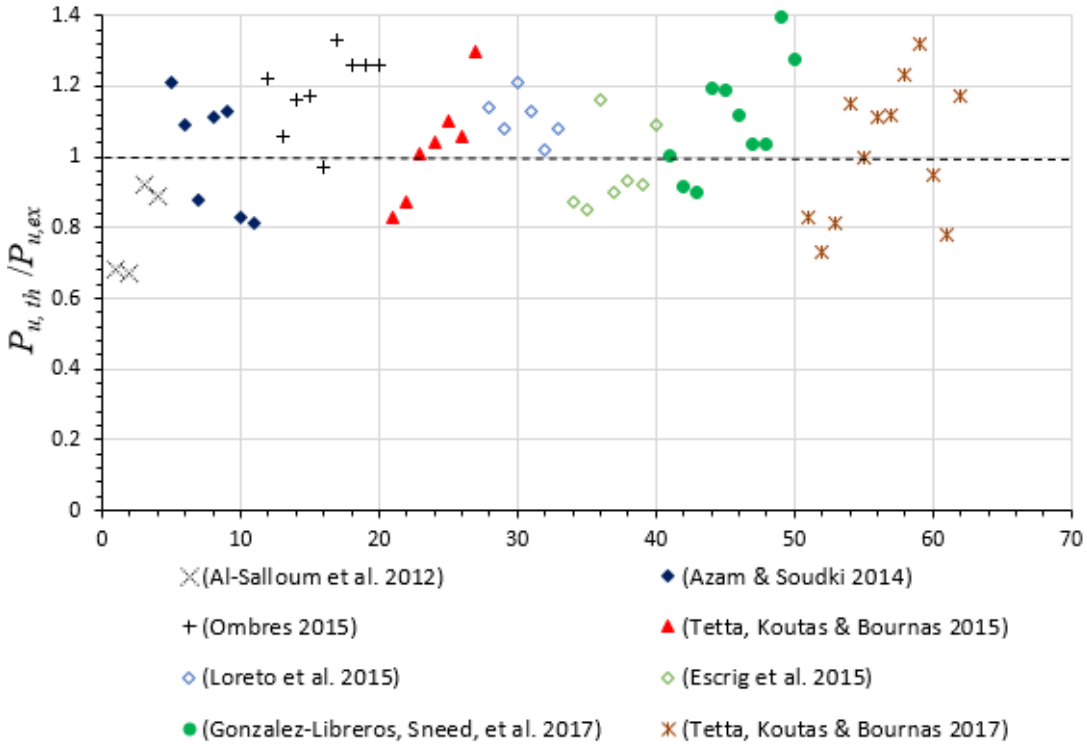

Figure 54: Verification of the model against the experimental data.

Table 10

Summary of the Theoretical and Experimental Results

Beam ID	Concrete			Internal reinforcement			Strengthening composite			Theoretical		$P_{u,ex}$ (kN)	$P_{u,th}/P_{u,ex}$
	f_c' (MPa)	b (mm)	d (mm)	f_{sv} (MPa)	ρ_{sv}	ρ_{sx}	Type	K_f (GPa)	ν (MPa)	V (kN)	$P_{u,th}$ (kN)		
Al-Salloum et al. [47]													
BS2	20	150	159	-	-	0.01317	B	0.2658	2.345	55.926	55.926	82.66	0.68
BS3	20	150	159	-	-	0.01317	B	0.2658	2.345	55.926	55.926	83.51	0.67
BS4	20	150	159	-	-	0.01317	B	0.5316	3.441	82.062	82.062	88.74	0.92
BS5	20	150	159	-	-	0.01317	B	0.5316	3.441	82.062	82.062	92.53	0.89
Azam and Soudki [52]													
C-N	38	150	307.5	-	-	0.0217	-	-	1.624	74.901	149.801	123.5	1.21
SB-GT	38	150	307.5	-	-	0.0217	G	0.0238	1.725	79.554	159.109	146.3	1.09
UW-GT	38	150	307.5	-	-	0.0217	G	0.0238	1.725	79.554	159.109	180.2	0.88
SB-CT1	38	150	307.5	-	-	0.0217	C	0.0563	1.865	86.037	172.074	155.5	1.11
UW-CT1	38	150	307.5	-	-	0.0217	C	0.0563	1.865	86.037	172.074	151.8	1.13
SB-CT2	38	150	307.5	-	-	0.0217	C	0.1354	2.213	102.094	204.188	245.4	0.83
UW-CT2	38	150	307.5	-	-	0.0217	C	0.1354	2.213	102.094	204.188	253.4	0.81

Table 10 (continued)

Summary of the Theoretical and Experimental Results

Beam ID	Concrete			Internal reinforcement			Strengthening composite			Theoretical		$P_{u,ex}$ (kN)	$P_{u,th}/P_{u,ex}$
	f_c' (MPa)	b (mm)	d (mm)	f_{sv} (MPa)	ρ_{sv}	ρ_{sx}	Type	K_f (GPa)	ν (MPa)	V (kN)	$P_{u,th}$ (kN)		
Ombres [59]													
TRA0	38.45	150	225	446.06	0.0023	0.0186	-	-	2.725	91.980	91.980	75.35	1.22
TRA1	38.45	150	225	446.06	0.0023	0.0186	PBO	0.0517	2.951	99.580	99.580	94.37	1.06
TRA2	38.45	150	225	446.06	0.0026	0.0186	PBO	0.0149	2.929	98.843	98.843	85.2	1.16
TRBO	56.275	150	224.82	446.06	0.0032	0.0279	-	-	3.671	123.804	123.804	105.7	1.17
TRB1	56.275	150	224.82	446.06	0.0032	0.0279	PBO	0.0777	4.020	135.578	135.578	139.53	0.97
TRB2	36.45	150	224.82	446.06	0.0032	0.0279	PBO	0.0777	3.783	127.559	127.559	95.83	1.33
TRB3	36.45	150	224.82	446.06	0.0032	0.0279	PBO	0.0370	3.595	121.243	121.243	95.93	1.26
TRB4	47.825	150	224.82	446.06	0.0032	0.0279	PBO	0.0370	3.742	126.185	126.185	99.98	1.26
TRB5	47.825	150	224.82	446.06	0.0032	0.0279	PBO	0.0370	3.742	126.185	126.185	99.88	1.26

Table 10 (continued)

Summary of the Theoretical and Experimental Results

Beam ID	Concrete			Internal reinforcement			Strengthening composite		Theoretical			$P_{u,ex}$	$P_{u,th}/P_{u,ex}$
	f_c' (MPa)	b (mm)	d (mm)	f_{sv} (MPa)	ρ_{sv}	ρ_{sx}	Type	K_f (GPa)	ν (MPa)	V (kN)	$P_{u,th}$ (kN)		
Tetta et al. [3]													
CON	21.6	102	177	-	-	0.02227	-	-	1.369	24.724	43.157	51.8	0.83
SB_M1	21.6	102	177	-	-	0.02227	C	0.0419	1.568	28.302	49.402	56.6	0.87
UW_M1	23.8	102	177	-	-	0.02227	C	0.2287	2.511	45.338	79.139	78.2	1.01
SB_M2	22.6	102	177	-	-	0.02227	C	0.3204	2.923	52.768	92.108	88.7	1.04
UW_M2	23.8	102	177	-	-	0.02227	C	0.5933	4.177	75.418	131.645	120.2	1.10
SB_M3	22.6	102	177	-	-	0.02227	C	0.4806	3.661	66.095	115.371	108.9	1.06
UW_M3	22.6	102	177	-	-	0.02227	C	0.8899	5.406	97.602	170.368	131.1	1.30
Loreto et al.[4]													
L_0_Ave	29.13	152	248	276	0.0027	0.0304	-	-	2.514	94.782	189.563	166.85	1.14
L_1_Ave	29.13	152	248	276	0.0027	0.0304	PBO	0.0794	2.903	109.413	218.826	203.13	1.08
L_4_Ave	29.13	152	248	276	0.0027	0.0304	PBO	0.3176	4.041	152.329	304.659	251.15	1.21
H_0_Ave	42.91	152	248	276	0.0027	0.0304	-	-	2.744	103.437	206.874	183.26	1.13
H_1_Ave	42.91	152	248	276	0.0027	0.0304	PBO	0.0794	3.119	117.577	235.154	231.17	1.02
H_4_Ave	42.91	152	248	276	0.0027	0.0304	PBO	0.3176	4.228	159.361	318.722	295.69	1.08

Table 10 (continued)

Summary of the Theoretical and Experimental Results

Beam ID	Concrete			Internal reinforcement			Strengthening composite		Theoretical				
	f_c' (MPa)	b (mm)	d (mm)	f_{sv} (MPa)	ρ_{sv}	ρ_{sx}	Type	K_f (GPa)	ν (MPa)	V (kN)	$P_{u,th}$ (kN)	$P_{u,ex}$ (kN)	$P_{u,th}/P_{u,ex}$
Escrig et al. [69]													
V-BR3-01	33.78	300	254	-	-	0.00792	B	0.0170	1.281	97.599	182.997	211.02	0.87
V-CXM25-01	33.78	300	254	-	-	0.00792	C	0.0251	1.309	99.747	187.025	220.42	0.85
V-CXM25-02	34.07	300	254	-	-	0.00792	C	0.0501	1.404	106.973	200.574	173.15	1.16
V-PXM750-01	34.07	300	254	-	-	0.00792	PBO	0.0388	1.362	103.797	194.618	215.95	0.90
V-PXM750-02	34.07	300	254	-	-	0.00792	PBO	0.0777	1.504	114.614	214.901	231.66	0.93
V-GPHDM-02	34.07	300	254	-	-	0.00792	G	0.0504	1.405	107.046	200.712	219.04	0.92
V-CONTROL	34.82	300	254	-	-	0.00792	-	-	1.234	94.065	176.371	161.59	1.09

Table 10 (continued)

Summary of the Theoretical and Experimental Results

Beam ID	Concrete			Internal reinforcement			Strengthening composite		Theoretical				
	f_c' (MPa)	b (mm)	d (mm)	f_{sv} (MPa)	ρ_{sv}	ρ_{sx}	Type	K_f (GPa)	ν (MPa)	V (kN)	$P_{u,th}$ (kN)	$P_{u,ex}$ (kN)	$P_{u,th}/P_{u,ex}$
Gonzalez-Libreros et al. [77]													
S1-CONTROL	23.3	150	230	527	0.0022	0.06156	-	-	3.356	115.793	231.586	230.5	1.00
S1-FRCM-F3-UN	23.3	150	230	527	0.0022	0.06156	C	0.0752	3.775	130.228	260.455	284.8	0.91
S1-FRCM-F3-UA	23.3	150	230	527	0.0022	0.06156	C	0.0752	3.775	130.228	260.455	290.3	0.90
S1-FRCM-F4-UN	21.3	150	230	527	0.0022	0.06156	C	0.342	5.180	178.697	357.394	299.5	1.19
S1-FRCM-F4-UA	21.3	150	230	527	0.0022	0.06156	C	0.342	5.180	178.697	357.394	300.3	1.19
S2-CONTROL	24.7	150	230	527	0.0034	0.06156	-	-	4.203	145.000	290.001	259.3	1.12
S2-FRCM-F3-UN	24.7	150	230	527	0.0034	0.06156	C	0.0752	4.611	159.094	318.187	307.9	1.03
S2-FRCM-F3-UA	24.7	150	230	527	0.0034	0.06156	C	0.0752	4.611	159.094	318.187	307.9	1.03
S2-FRCM-F4-UN	21.3	150	230	527	0.0034	0.06156	C	0.342	5.955	205.440	410.880	294.4	1.40
S2-FRCM-F4-UA	21.3	150	230	527	0.0034	0.06156	C	0.342	5.955	205.440	410.880	321.9	1.28

Table 10 (continued)

Summary of the Theoretical and Experimental Results

Beam ID	Concrete			Internal reinforcement			Strengthening composite		Theoretical				
	$f_c{}'$ (MPa)	b (mm)	d (mm)	f_{sv} (MPa)	ρ_{sv}	ρ_{sx}	Type	K_f (GPa)	ν (MPa)	V (kN)	$P_{u,th}$ (kN)	$P_{u,ex}$ (kN)	$P_{u,th}/P_{u,ex}$
Tetta et al. [92]													
CON	21.6	102	177	-	-	0.022	-	-	1.365528	24.6532	43.0333	51.8	0.83
CL1	23	102	177	-	-	0.022	C	0.2038	2.370672	42.8001	74.7094	102.3	0.73
CL1 STRIPS	20	102	177	-	-	0.022	C	0.3122	2.82976	51.0885	89.1772	110.7	0.81
CH1	23.8	102	177	-	-	0.022	C	0.3042	2.860386	51.6414	90.1423	78.2	1.15
CH1_CL1	20	102	177	-	-	0.022	C	0.5079	3.731802	67.3739	117.604	117.4	1.00
CH2	23.8	102	177	-	-	0.022	C	0.6084	4.23326	76.4273	133.407	120.2	1.11
CL3	20.8	102	177	-	-	0.022	C	0.6113	4.199244	75.8131	132.335	118	1.12
CH2_CL1	20	102	177	-	-	0.022	C	0.8121	5.037996	90.956	158.768	129.3	1.23
CH3	22.6	102	177	-	-	0.022	C	0.9126	5.482162	98.9749	172.765	131.1	1.32
CON_3.6	20.5	102	177	-	-	0.022	-	-	1.338383	24.1632	58.8772	62.2	0.95
CL1_3.6	22.6	102	177	-	-	0.022	C	0.2038	2.362129	42.6459	103.913	133.8	0.78
CL3_3.6	22.6	102	177	-	-	0.022	C	0.6113	4.228096	76.334	185.999	158.7	1.17

CHAPTER 6: SUMMARY AND CONCLUSION

This thesis presents an experimental study on the efficacy of FRCM system using the new forms of NSE-FRCM and hybrid NSE/EB-FRCM techniques for shear strengthening of RC beams. For this purpose, twenty (20) shear deficient RC beams have been prepared and tested under three-point bending at a displacement rate of 0.25 mm/min. Moreover, the interaction between the TSR and the FRCM system has been investigated. The experimental results have been discussed in terms of the ultimate load carrying capacity, deformation and ductility characteristics, modes of failure, crack width, and strains. Different commercially available fabric types were used with their respective manufacturer recommended types of mortar. Therefore, the test parameters were: (a) type of FRCM, (b) strengthening configuration, and (c) presence of the transverse shear reinforcement. Moreover, the effect of additional two layers of externally bonded FRCM system on the NSE-FRCM system has been studied in the technique that is referred to as hybrid NSE/EB-FRCM. The main conclusions drawn from this study are summarized as follows.

- FRCM can be used to significantly increase the load carrying capacity of shear deficient RC beams in both the NSE-FRCM and hybrid NSE/EB-FRCM techniques. An enhancement in the ultimate load carrying capacity ranging from 14% to 77% was observed in NSE-FRCM system, while an increment ranging from 63% to 114% was observed in hybrid NSE/EB-FRCM system.
- With regard to the FRCM type, C-FRCM strengthening system performed better than G-FRCM system, while G-FRCM in turn performed better than PBO-FRCM

system in enhancing the ultimate load carrying capacity of the strengthened specimens.

- With regard to the FRCM configuration, full FRCM configuration has shown to be more effective than intermittent configuration for the FRCM system indicating the effectiveness of the FRCM continuity and quantity in enhancing the load carrying capacity of the beams.
- The efficacy of the FRCM system was reduced by the presence of the TSR within the CSS. An average overall gain in the ultimate load carrying capacity was reduced from 59.5% observed for beams without TSR within the CSS to 30.7% for beams with TSR.
- The strengthening system improved the deformational characteristics of the strengthened specimens relative to the benchmarks in both the NSE and the hybrid NSE/EB techniques. For the NSE-FRCM system, an average increase in the deflection at the ultimate load were 67% and 44% for the specimens without and with TSR within the CSS, respectively. Moreover, the average gains in energy absorption were 143% and 67% relative to the benchmarks for the specimens without and with TSR within the CSS, respectively.
- The interaction between the NSE-FRCM system and TSR has been observed. The NSE-FRCM strengthening system reduced the strains in the TSR relative to the reference specimen.
- The NSE technique improved the FRCM/concrete bond; hence, increasing the utilization of the FRCM system. Generally, FRCM/concrete debonding failure was

mitigated. An addition of two layers of EB-FRCM system on the NSE-FRCM system changed the failure mode to the debonding of FRCM off the concrete substrate in the hybrid NSE/EB-FRCM system.

- With regard to the number of FRCM layers, provision of additional two layers of EB-FRCM system increased the ultimate load carrying capacity of the strengthened specimen relative to those using only the two layers of NSE-FRCM system. However, the increase in the ultimate load carrying capacity was not proportional to the number of FRCM layers. This disproportionality was caused by the debonding of FRCM initiated by the additional two layers of EB-FRCM system.
- Finally, an analytical approach has been proposed to predict the ultimate load carrying capacity of the FRCM strengthened specimens based on the simplified compression field theory (SCFT). Over sixty test results of RC beams obtained from the literature in addition to the NSE-FRCM specimens have been used to validate the proposed model. The results indicated that the model can reasonably predict the ultimate load carrying capacity of the FRCM strengthened specimens.
- Additional research contributions are required to investigate the efficacy of the NSE-FRCM and the hybrid NSE/EB-FRCM systems under fatigue loading.

CHAPTER 7: REFERENCES

[1] Younis A, Ebead U, Shrestha K. Different FRCM systems for shear-strengthening of reinforced concrete beams. Constr Build Mater 2017;153:514–26.

[2] Oluwafunmilayo A, El-Maaddawy T, Ismail N. Fabric-reinforced cementitious matrix: A promising strengthening technique for concrete structures. Constr Build Mater 2017;132:94–111. doi:10.1016/j.conbuildmat.2016.11.125.

[3] Tetta Z, Koutas L, Bournas D. Textile-reinforced mortar (TRM) versus fiber-reinforced polymers (FRP) in shear strengthening of concrete beams. Compos Part B 2015;77:338–48. doi:10.1016/j.compositesb.2015.03.055.

[4] Loreto G, Babaeidarabad S, Leardini L, Nanni A. RC beams shear-strengthened with fabric-reinforced-cementitious-matrix (FRCM) composite. Int J Adv Struct Eng 2015;7:341–52. doi:10.1007/s40091-015-0102-9.

[5] Jacketing Concrete Column n.d. http://www.pinsdaddy.com/jacketing-concrete-column_chssarMWB7IxCaM2LsT%7Ct3E3MXTCw9V7IA3OUoTGh2k/.

[6] Aravinthan T. Is external post-tensioning an effective solution for shear strengthening of bridge elements. Univ South Queensl Fac Eng Surv Toowoomba QLD 4350 Aust 2006.

[7] Alkhrdaji T, Thomas J. Structural Strengthening Using External Post-Tensioning Systems. Struct Mag 2009:8–10.

[8] ICRI. Guideline for the Selection of Strengthening Systems for Concrete Structures, Guideline No. 03742 2006:32.

[9] Alkhrdaji T. Design and Application Techniques Key to Successful Structural Strengthening Projects n.d. www.structural.net/article/design-and-application-

techniques-key-successful-structural-strengthening-projects.

[10] Ashour AF, El-Refaie SA, Garrity SW. Flexural strengthening of RC continuous beams using CFRP laminates. Cem Concr Compos 2004;26:765–75. doi:10.1016/j.cemconcomp.2003.07.002.

[11] Attari N, Amziane S, Chemrouk M. Flexural strengthening of concrete beams using CFRP, GFRP and hybrid FRP sheets. Constr Build Mater 2012;37:746–57. doi:10.1016/j.conbuildmat.2012.07.052.

[12] Ebead U, Saeed H. Flexural and Interfacial Behavior of Externally Bonded/ Mechanically Fastened Fiber-Reinforced Polymer Strengthened Reinforced Concrete Beams. ACI Struct J 2014;111. doi:10.14359/51686628.

[13] Kotynia R, Abdel Baky H, Neale K, Ebead U. Flexural strengthening of RC beams with externally bonded CFRP systems: Test results and 3D nonlinear FE analysis. J Compos Constr 2008;12:190–201. doi:10.1061/(ASCE)1090-0268(2008)12:2(190).

[14] Ebead U, Saeed H. FRP/stirrups interaction of shear-strengthened beams. Mater Struct 2017;50:103. doi:10.1617/s11527-016-0973-7.

[15] Ebead U. Hybrid externally bonded/mechanically fastened fiber-reinforced polymer for RC beam strengthening. ACI Struct J 2012;108:669–78.

[16] Ebead U, Saeed H. Hybrid shear strengthening system for reinforced concrete beams : An experimental study. Eng Struct 2013;49:421–33. doi:10.1016/j.engstruct.2012.11.039.

[17] Smith ST, Kim SJ. Strengthening of one-way spanning RC slabs with cutouts using FRP composites. Constr Build Mater 2009;23:1578–90.

doi:10.1016/j.conbuildmat.2008.06.005.

[18] Al-Rousan R, Issa M, Shabila H. Performance of reinforced concrete slabs strengthened with different types and configurations of CFRP. Compos Part B Eng 2012;43:510–21. doi:10.1016/j.compositesb.2011.08.050.

[19] Siddiqui NA, Alsayed S, Al-Salloum Y, Iqbal RA, Abbas H. Experimental investigation of slender circular RC columns strengthened with FRP composites. Constr Build Mater 2014;69:323–34. doi:10.1016/j.conbuildmat.2014.07.053.

[20] Pham TM, Doan L V., Hadi MNS. Strengthening square reinforced concrete columns by circularisation and FRP confinement. Constr Build Mater 2013;49:490–9. doi:10.1016/j.conbuildmat.2013.08.082.

[21] Mirmiran A, Shahawy M, Samaan M, Echary HE, Mastrapa JC, Pico O. Effect of column parameters on FRP-confined concrete. J Compos Constr 1998;2:175–85.

[22] Panigrahi AK, Biswal KC, Barik MR. Strengthening of shear-deficient RC T-beams with externally bonded GFRP sheets. Constr Build Mater 2014;57:81–91. doi:10.1016/j.conbuildmat.2014.01.076.

[23] El-Maaddawy T, Chekfeh Y. Shear strengthening of T-beams with corroded stirrups using composites. ACI Struct J 2013;110:779–89.

[24] El-Maaddawy T, Chekfeh Y. Retrofitting of severely shear-damaged concrete T-beams using externally bonded composites and mechanical end anchorage. J Compos Constr 2012;16:693–704. doi:10.1061/(ASCE)CC.1943-5614.0000299.

[25] Wang Q, Guan Z. CFRP sheets for flexural strengthening of RC beams. Compos Part B 2011;44:604–12. doi:10.1016/j.compositesb.2012.02.018.

[26] Ebead U, Neale KW. Mechanics of fibre-reinforced polymer - concrete interfaces.

Can J Civ Eng 2007;34:367–77. doi:10.1139/l06-107.

[27] Ali, Ragy; Benmokrane, Brahim, Ebead U. Tensile lap splicing of bundled CFRP reinforcing bars in concrete. J Compos Constr 2012;10:2012. doi:10.1061/(ASCE)1090-0268(2006)10.

[28] Neale KW, Godat A, Abdel Baky HM, Elsayed WE, Ebead UA. Approaches for Finite Element Simulations of Frp-Strengthened Concrete Beams and Slabs. Archit Civ Eng Environ 2011;4:59–72.

[29] Dias SJE, Barros JAO. NSM shear strengthening technique with CFRP laminates applied in high-strength concrete beams with or without pre-cracking. Compos Part B Eng 2012;43:290–301. doi:10.1016/j.compositesb.2011.09.006.

[30] Rizzo A, Lorenzis L. Behavior and capacity of RC beams strengthened in shear with NSM FRP reinforcement. Constr Build Mater 2009;23:1555–67. doi:10.1016/j.conbuildmat.2007.08.014.

[31] Lorenzis L De, Teng JG. Near-surface mounted FRP reinforcement : An emerging technique for strengthening structures. Compos Part B 2007;38:119–43. doi:10.1016/j.compositesb.2006.08.003.

[32] Barros JAO, Dias SJE. Near surface mounted CFRP laminates for shear strengthening of concrete beams. Cem Concr Compos 2006;28:276–92. doi:10.1016/j.cemconcomp.2005.11.003.

[33] Lorenzis L, Nanni A. Shear srengthening of reinforced concrete beams with near-surface mounted fiber reinforced polymer rods. ACI Struct J 2001;98 No.1.

[34] Almusallam T, Elsanadedy H, Al-Salloum Y, Alsayed S. Experimental and numerical investigation for the flexural strengthening of RC beams using near-

surface mounted steel or GFRP bars. Constr Build Mater 2013;40:145–61. doi:10.1016/j.conbuildmat.2012.09.107.

[35] Sharaky IA, Torres L, Comas J, Barris C. Flexural response of reinforced concrete (RC) beams strengthened with near surface mounted (NSM) fibre reinforced polymer (FRP) bars. Compos Struct 2014;109:8–22. doi:10.1016/j.compstruct.2013.10.051.

[36] Elsayed W, Ebead U, Neale K. Studies on mechanically fastened fiber-reinforced polymer strengthening systems. ACI Struct J 2009;106:49–59.

[37] Grelle S V., Sneed L. Review of anchorage systems for externally bonded FRP laminates. Int J Concr Struct Mater 2013;7:17–33. doi:10.1007/s40069-013-0029-0.

[38] Lorenzis L, Nanni A. Contribution of NSM CFRP bars in shear strengthening of concrete members. 2010 Taylor Fr Gr 2002:221–8.

[39] A.K.M. Anwarul Islam. Effective methods of using CFRP bars in shear strengthening of concrete girders. Eng Struct 2009;31:709–14. doi:10.1016/j.engstruct.2008.11.016.

[40] Al-Mahmoud F, Castel A, Trinh Quang Minh, Francois R. Reinforced concrete beams strengthened with NSM CFRP rods in shear. Adv Struct Eng 2015;18:1563–74.

[41] Dias SJE, Barros JAO. Performance of reinforced concrete T-beams strengthened in shear with NSM CFRP laminates. Eng Struct 2010;32:373–84. doi:10.1016/j.engstruct.2009.10.001.

[42] Hassan T, Rizkalla S. Investigation of bond in concrete structures strengthened

with near surface mounted carbon fiber reinforced polymer strips. J Compos Constr 2003;7:248–57. doi:10.1061/(ASCE)1090-0268(2003)7:3(248).

[43] Bilotta A, Ceroni F, Di Ludovico M, Nigro E, Pecce M, Manfredi G. Bond efficiency of EBR and NSM FRP systems for strengthening concrete members. J Compos Constr 2011;15:757–72. doi:10.1061/(ASCE)CC.1943-5614.0000204.

[44] Triantafillou T, Papanicolaou C. Shear strengthening of reinforced concrete members with textile reinforced mortar (TRM) jackets. Mater Struct 2006;39:93–103. doi:10.1617/s11527-005-9034-3.

[45] Raoof S, Bournas D. TRM versus FRP in flexural strengthening of RC beams: Behaviour at high temperatures. Constr Build Mater 2017;154:424–37. doi:10.1016/j.conbuildmat.2017.07.195.

[46] Tetta Z, Bournas D. TRM vs FRP jacketing in shear strengthening of concrete members subjected to high temperatures. Compos Part B 2016;106:190–205. doi:10.1016/j.compositesb.2016.09.026.

[47] Al-Salloum Y, Elsanadedy H, Alsayed S, Iqbal RA. Experimental and numerical study for the shear strengthening of reinforced concrete beams using textile-reinforced mortar. J Compos Constr 2012;16:74–90. doi:10.1061/(ASCE)CC.1943-5614.0000239.

[48] Ebead U, Shrestha K, Afzal M, Refai A, Nanni A. Effectiveness of fabric-reinforced cementitious matrix in strengthening reinforced concrete beams. J Compos Constr 2017;21:4016084. doi:10.1061/(ASCE)CC.1943-5614.0000741.

[49] Trapko T, Urbańska D, Kamiński M. Shear strengthening of reinforced concrete beams with PBO-FRCM composites. Compos Part B 2015;80:63–72.

doi:10.1016/j.compositesb.2015.05.024.

[50] Täljsten B, Blanksvärd T. Mineral-based bonding of carbon FRP to strengthen concrete structures. J Compos Constr 2007;11:120–8. doi:10.1061/(ASCE)1090-0268(2007)11:2(120).

[51] Raoof S, Koutas L, Bournas D. Textile-reinforced mortar (TRM) versus fibre-reinforced polymers (FRP) in flexural strengthening of RC beams. Constr Build Mater 2017;151:279–91. doi:10.1016/j.conbuildmat.2017.05.023.

[52] Azam R, Soudki K. FRCM strengthening of shear-critical RC beams. J Compos Constr 2014;18:1–9. doi:10.1061/(ASCE)CC.1943-5614.0000464.

[53] Tetta Z, Koutas L, Bournas D. Shear strengthening of full-scale RC T-beams using textile-reinforced mortar and textile-based anchors. Compos Part B 2016;95:225–39. doi:10.1016/j.compositesb.2016.03.076.

[54] Younis, Adel; Ebead U. Bond characteristics of different FRCM systems. Constr Build Mater 2018;175:610–20. doi:10.1016/j.conbuildmat.2018.04.216.

[55] Shrestha KC, Ebead U, Younis A. Effect of Surface Roughening on Concrete/TRM Bond. Proc. Ninth Int. Struct. Eng. Constr. Conf. Resilient Struct. Sustain. Constr., Valencia, Spain: ISEC Press; 2017, p. St--43.

[56] Si Larbi A, Contamine R, Ferrier E, Hamelin P. Shear strengthening of RC beams with textile reinforced concrete (TRC) plate. Constr Build Mater 2010;24:1928–36. doi:10.1016/j.conbuildmat.2010.04.008.

[57] Oluwafunmilayo A, E l-Maaddawy T, Refai A. Numerical simulation and experimental testing of concrete beams strengthened in shear with fabric-reinforced cementitious matrix. J Compos Constr 2015;20:1–11.

doi:10.1061/(ASCE)CC.1943-5614.0000711.

[58] Contamine R, Si Larbi A, Hamelin P. Identifying the contributing mechanisms of textile reinforced concrete (TRC) in the case of shear repairing damaged and reinforced concrete beams. Eng Struct 2013;46:447–58. doi:10.1016/j.engstruct.2012.07.024.

[59] Ombres L. Structural performances of reinforced concrete beams strengthened in shear with a cement based fiber composite material. Compos Struct 2015;122:316–29. doi:10.1016/j.compstruct.2014.11.059.

[60] Azam R, Soudki K, West J, Noël M. Strengthening of shear-critical RC beams: Alternatives to externally bonded CFRP sheets. Constr Build Mater 2017;151:494–503. doi:10.1016/j.conbuildmat.2017.06.106.

[61] Younis A, Ebead U, Shrestha KC. FRCM Shear Strengthening for Concrete Beams. Proc. Ninth Int. Struct. Eng. Constr. Conf. Resilient Struct. Sustain. Constr., Valencia, Spain: ISEC Press; 2017, p. St--27.

[62] Escrig C, Gil L, Bernat-maso E. Experimental comparison of reinforced concrete beams strengthened against bending with different types of cementitious-matrix composite materials. Constr Build Mater 2017;137:317–29. doi:10.1016/j.conbuildmat.2017.01.106.

[63] D'Ambrisi A, Focacci F. Flexural strengthening of RC beams with cement-based composites. J Compos Constr 2011;15:707–20. doi:10.1061/(ASCE)CC.1943-5614.0000218.

[64] Elghazy M, Refai A, Ebead U, Nanni A. Effect of corrosion damage on the flexural performance of RC beams strengthened with FRCM composites. Compos

Struct 2017;180:994–1006. doi:10.1016/j.compstruct.2017.08.069.

[65] Alabdulhady MY, Sneed L, Carloni C. Torsional behavior of RC beams strengthened with PBO-FRCM composite – An experimental study. Eng Struct 2017;136:393–405. doi:10.1016/j.engstruct.2017.01.044.

[66] Ludovico M, Prota A, Manfredi G. Structural upgrade using basalt fibers for concrete confinement. J Compos Constr 2010;14:541–52. doi:10.1061/(ASCE)CC.1943-5614.0000114.

[67] Peled A. Confinement of damaged and nondamaged structural concrete with FRP and TRC sleeves. J Compos Constr 2007;11:514–22.

[68] Triantafillou T, Papanicolaou C, Zissimopoulos P, Laourdekis T. Concrete confinement with textile-reinforced mortar jackets. ACI Struct J 2006;103:28–37.

[69] Escrig C, Gil L, Bernat-Maso E, Puigvert F. Experimental and analytical study of reinforced concrete beams shear strengthened with different types of textile-reinforced mortar. Constr Build Mater 2015;83:248–60. doi:10.1016/j.conbuildmat.2015.03.013.

[70] Brückner A, Ortlepp R, Curbach M. Anchoring of shear strengthening for T-beams made of textile reinforced concrete (TRC). Mater Struct 2008;41:407–18. doi:10.1617/s11527-007-9254-9.

[71] Babaeidarabad S, Loreto G, Nanni A. Flexural strengthening of RC beams with an externally bonded fabric-reinforced cementitious matrix. J Compos Constr 2014;18:1–12. doi:10.1061/(ASCE)CC.1943-5614.0000473.

[72] Jabr A, El-Ragaby A, Ghrib F. Effect of the fiber type and axial stiffness of FRCM on the flexural strengthening of RC beams. Fibers 2017;5:2.

doi:10.3390/fib5010002.

[73] Pino V, Hadad H, Basalo F, Nanni A, Ebead U, Refai A. Performance of FRCM-strengthened RC beams subject to fatigue. J Bridg Eng 2017;22:4017079. doi:10.1061/(ASCE)BE.1943-5592.0001107.

[74] Elghazy M, El Refai A, Ebead U, Nanni A. Post-repair flexural performance of corrosion-damaged beams rehabilitated with fabric-reinforced cementitious matrix (FRCM). Constr Build Mater 2018;166:732–44. doi:10.1016/j.conbuildmat.2018.01.128.

[75] Blanksvärd T, Täljsten B, Carolin A. Shear strengthening of concrete structures with the use of mineral-based composites. J Compos Constr 2009;13:25–34. doi:10.1061/(ASCE)1090-0268(2009)13:1(25).

[76] Tzoura E, Triantafillou T. Shear strengthening of reinforced concrete T-beams under cyclic loading with TRM or FRP jackets. Mater Struct 2014;49:17–28. doi:10.1617/s11527-014-0470-9.

[77] Gonzalez-Libreros JH, Sneed L, D'Antino T, Pellegrino C. Behavior of RC beams strengthened in shear with FRP and FRCM composites. Eng Struct 2017;150:830–42. doi:10.1016/j.engstruct.2017.07.084.

[78] Aljazaeri Z, Myers J. Strengthening of reinforced concrete beams in shear with a fabric-reinforced cementitious matrix. J Compos Constr 2017;21:1–11. doi:10.1061/(ASCE)CC.1943-5614.0000822.

[79] Ombres L. Debonding analysis of reinforced concrete beams strengthened with fibre reinforced cementitious mortar. Eng Fract Mech 2012;81:94–109. doi:10.1016/j.engfracmech.2011.06.012.

[80] Oluwafunmilayo A, El-Maaddawy T, Refai A El. Numerical Simulation and Experimental Testing of Concrete Beams Strengthened in Shear with Fabric-Reinforced Cementitious Matrix. J Compos Constr 2015:1–11. doi:10.1061/(ASCE)CC.1943-5614.0000711.

[81] Gonzalez-Libreros JH, Sabau C, Sneed L, Pellegrino C, Sas G. State of research on shear strengthening of RC beams with FRCM composites. Constr Build Mater 2017;149:444–58. doi:10.1016/j.conbuildmat.2017.05.128.

[82] ASTM International ASTM C39/C39M-16b. Standard test method for compressive strength of cylindrical concrete specimens, ASTM International, West Conshohocken, PA, 2016. 2009.

[83] 4449:2005 B, Committee I. BS 4449:2005: Steel for the reinforcement of concrete. Weldable reinforcement steel. Bar, coil and decoiled product. BSI, 2005 n.d.

[84] Ruredil, Technical datasheet. Ruredil X Mesh Gold n.d.

[85] SIKA Technical datasheet. SikaWrap-350G Grid data sheet, 2016. n.d.

[86] Ruredil, Technical datasheet. X MESH C10 RUREDIL X MESH C10 2013:1–6.

[87] Li A, Cheikhna Diagana, Delmas Y. CRFP contribution to shear capacity of strengthened RC beams. Eng Struct 2001;23:1212–20. doi:10.1016/S0141-0296(01)00035-9.

[88] Vecchio FJ, Collins MP. The modified compression-field theory for reinforced concrete elements subjected to shear. ACI J Proc 1986;83. doi:10.14359/10416.

[89] Bentz EC, Vecchio FJ, Collins MP. Simplified modified compression field theory for calculating shear strength of reinforced concrete elements. ACI Struct J 2006;103:614–24.

[90] ACI Committee 549. Guide to design and construction of externally bonded fabric-reinforced cementitious matrix (FRCM) systems for repair and strengthening concrete and masonry structures (ACI 549.4R-13). American Concrete Institute, Farmington Hills, MI, USA.; 2013.

[91] Joint ACI-ASCE Committee 445. Recent approaches to shear design of structural concrete. J Struct Eng 1998;124:1374–417. doi:10.1061/(ASCE)0733-9445(1998)124:12(1375).

[92] Tetta Z, Koutas L, Bournas D. Shear strengthening of concrete members with TRM jackets: Effect of shear span-to-depth ratio, material and amount of external reinforcement. Compos Part B Eng 2017;137:184–201. doi:10.1016/j.compositesb.2017.10.041.